Testing the universality of star formation - I. Multiplicity in nearby star-forming regions

Robert R. King[1]⋆, Richard J. Parker[2,3], Jenny Patience[1], and Simon P. Goodwin[3]

[1] *Astrophysics Group, College of Engineering Mathematics and Physical Sciences, University of Exeter, Stocker Road, Exeter EX4 4QL, UK*
[2] *Institute of Astronomy, ETH Zürich, Wolfgang-Pauli-Strasse 27, 8093 Zürich, Switzerland*
[3] *Department of Physics and Astronomy, University of Sheffield, Hicks Building, Hounsfield Road, Sheffield, S3 7RH, UK*

ABSTRACT

We have collated multiplicity data for five clusters (Taurus, Chamaeleon I, Ophiuchus, IC348, and the Orion Nebula Cluster). We have applied the same mass ratio (flux ratios of $\Delta K \leq 2.5$) and primary mass cuts (~ 0.1–$3.0\,M_\odot$) to each cluster and therefore have directly comparable binary statistics for all five clusters in the separation range 62–620 au, and for Taurus, Chamaeleon I, and Ophiuchus in the range 18–830 au. We find that the trend of decreasing binary fraction with cluster density is solely due to the high binary fraction of Taurus, the other clusters show no obvious trend over a factor of nearly 20 in density.

With N-body simulations we attempt to find a set of initial conditions that are able to reproduce the density, morphology and binary fractions of all five clusters. Only an initially clumpy (fractal) distribution with an initial total binary fraction of 73 per cent (17 per cent in the range 62–620 au) is able to reproduce all of the observations (albeit not very satisfactorily). Therefore, if star formation is universal the initial conditions must be clumpy and with a high (but not 100 per cent) binary fraction. This could suggest that most stars, including M-dwarfs, form in binaries.

Key words: stars: binaries – formation – kinematics – galaxy: open clusters and associations - methods: numerical

1 INTRODUCTION

Star formation is one of the outstanding problems in astrophysics. How stars form is extremely interesting in itself, but also has huge implications for understanding galaxy formation and evolution, and planet formation.

One of the major unsolved problems in star formation is the universality of the process: is the difference between small, local star forming regions such as Taurus ($\sim 10^2 M_\odot$), and massive starburst clusters like 30 Doradus ($\sim 10^5 M_\odot$) merely one of the level of star formation, or is there something fundamentally different between these two extremes?

There is no evidence that the initial mass function (IMF) of stars varies systematically between different environments (see e.g., Luhman et al. 2003; Bastian et al. 2010). Such a result is rather surprising and interesting, but it means that determinations of the IMF are unable to probe the universality, or otherwise, of star formation. A more promising route might be to search for differences between *primordial* binary populations – if two regions pro-

duce very different binary populations then this suggests that star formation was different between these regions (see Duchêne et al. 2004; Goodwin 2010).

Indeed, differences between the binary populations of different clusters have been observed. Most famously, the binary fraction of Taurus (Leinert et al. 1993) is significantly higher than the binary fraction of the Orion Nebula Cluster (hereafter ONC, Prosser et al. 1994; Petr et al. 1998; Köhler et al. 2006; Reipurth et al. 2007) and approximately twice that seen in the field (Duquennoy & Mayor 1991; Fischer & Marcy 1992; Raghavan et al. 2010).

However, we know that dense regions will process their primordial binary populations and what we see at later times may not reflect the primordial population. In a dense environment encounters are common and binaries will tend to be destroyed (Heggie 1975; Hills 1975). Kroupa (1995a,b) showed that it is possible to process a Taurus-like primordial binary population into an Orion-like evolved population very quickly. However, Parker, Goodwin & Allison (2011) suggest that even with dynamical processing the primordial binary populations of Taurus and the ONC were probably

⋆ E-mail: rob@astro.ex.ac.uk

different (see also Kroupa & Petr-Gotzens 2011; Marks et al. 2011).

The problem is that it is difficult to 'reverse engineer' the current binary population of a cluster to determine the primordial population (reverse population synthesis, Kroupa 1995b). A major aspect of this problem is that it is difficult to compare the observed binary populations of different regions due to differences in the separation range probed and the sensitivity to lower-mass companions between different surveys.

In this paper we approach the problem of examining differences between primordial binary populations with a two-fold approach. Firstly, we construct (in as much as is possible) a uniform comparison of binary fractions in the same separation ranges for five different regions (Taurus, Oph/L1688, Cham I, IC348, and the ONC). Secondly, we attempt to simulate their dynamical evolution and binary destruction as realistically as possible with both smooth and clumpy initial conditions.

This paper is organised as follows. In Section 2 we describe the observations of binarity that we have used in our five different regions. In Section 3 we construct as fair a comparison as possible between the regions. We summarise these results and discuss the structure of each cluster in Section 4. In Section 5 we introduce our *N*-body simulations and compare these with the observational results. In Section 6 we discuss our findings, finally concluding in Section 7.

2   CLUSTER MEMBERSHIPS AND BINARITY

We have chosen to compare binary surveys of young stars in five well-studied regions: the Chamaeleon I cloud (Lafrenière et al. 2008), Taurus (Leinert et al. 1993), L1688 in Ophuichus (Ratzka et al. 2005), IC348 (Duchêne et al. 1999) and the Orion Nebula Cluster (Reipurth et al. 2007). The first four of these surveys all involved near-IR observations (3 *K*-band, 1 *H*-band) and so are most easily compared. The fifth survey (of the ONC) was selected because it is the most comprehensive survey of this important, massive star-formation region. These regions provide as broad a range in density as possible within the confines of the Solar Neighbourhood which allows us to probe down to separations of a few tens of au.

After summarising the most important past studies for each region, we identify the most comprehensive binary studies with which we will make a comparison between the different regions. For each region we report the multiplicity fraction (MF) and the corresponding companion star fraction (CSF) defined as

$$MF = \frac{B + T + Q}{S + B + T + Q} \qquad (1)$$

$$CSF = \frac{B + 2T + 3Q}{S + B + T + Q} \qquad (2)$$

where S is the number of single stars, B, T and Q are the numbers of binary, triple and quadruple systems, respectively. Our *N*-body simulations do not produce systems with more than two components, so in this case the MF and CSF are equal to the binary fraction.

For each of the five star-forming regions we also report

Table 1. A summary of the number of stars and densities calculated for each region.

Region	# of Stellar Members	Stellar Density (stars pc^{-3})		
		$r_{1/2}$	r<0.25 pc	r<0.10 pc
Cham I	200	5.7±0.7	275±65	1190±530
Taurus	215	—	6.0±1.2	—
Oph	295	236±27	610±180	1910±955
IC 348	265	326±73	1115±140	3820±1110
ONC	~1700	425±33	4700±290	22600±1200

Note: The density reported here for Taurus is calculated within a radius of 1 pc from the centre of L1495; the number of stellar members for the ONC is extrapolated from the number of COUP sources within the half-number radius ($r_{1/2}$) defined using the Hillenbrand (1997) survey; and the number of stellar members for Taurus is for the Northern filament only.

the most recent determinations of the stellar membership. With these data we form a rough estimate of the stellar densities. Note that to ensure consistency we exclude brown dwarfs from the density calculation and focus on the more easily identified stellar population.

We measure the number of stars within the half-number, 0.1 pc and 0.25 pc radii from a cluster 'centre' determined from the average ('centre of mass') positions of all the stars. We then assume that the third dimension is the same allowing us a basic estimate of the stellar volume densities in each region as shown in Table 1. The uncertainties on the densities are estimated by accounting for the Poisson errors on the stars within each volume and the uncertainty on the distance to each region. As we will see later in Section 4.2, several of these regions are far from spherical and lack a proper 'centre'. However, we feel that these approximate densities give a broad picture of the relative densities.

2.1   Chamaeleon I

2.1.1   Membership

To estimate the density of the young stellar cluster Cham I, we have used the compilation of known members presented by Luhman (2008). This member list was constructed from the results of many past studies including surveys for Hα emission, X-ray emission, photometric variability and IR-excess emission. There have also been Cham I members identified using optical and near-IR imaging, due to the moderate optical extinction, and the subsequent colour-magnitude diagram position of members relative to the contamination.

The known members include brown dwarfs with spectral types as late as M9.5. At the cluster age of ~2 Myr (Luhman 2004, 2007), the sub-stellar limit occurs at an approximate spectral type of M6. From the total of 237 known members of Cham I, we are left with 201 stellar members after removing those with spectral types later than M6 (as reported by Luhman (2008))

At an age of 2 Myr, a 0.1 $M_\odot$ star is expected to have an apparent magnitude of $K_S \simeq 11$ at the distance of Cham I. Given the 2MASS 10-σ detection limit ($K_S \simeq 14.3$), we would expect 2MASS to have detected all stars through A$_V$<30, much larger than the estimated maximum extinction in Cham I of A$_V$ =5–10. Additionally, from a very sensitive X-ray observation of the northern cluster of Cham I, Feigel-

Table 2. A summary of the separation ranges, contrasts and derived multiplicity fractions from each binary survey used.

Region	Separation Range (arcsec)	(au)	Contrast	Multiplicity Fraction	Reference
Taurus	0.13–13.	18–1820	$\Delta K \leq 2.5$	42±8%	Leinert et al. (1993)
Oph/L1688	0.13–6.4	17–830	$\Delta K \leq 2.5$	31±6%	Ratzka et al. (2005)
Cham I	0.10–6.0	16–960	$\Delta K \leq 3.1$	$27\pm^{5}_{4}\%$	Lafrenière et al. (2008)
IC 348	0.10–8.0	32–2530	$\Delta H \leq 6.5$	20±5%	Duchêne et al. (1999)
ONC	0.15–1.5	62–620	$\Delta H\alpha \leq 5.0$	8.5±1.0%	Reipurth et al. (2007)

son & Lawson (2004) found no evidence for previously unreported members suggesting the known members in that field are complete to $0.1\,M_\odot$. We therefore consider the membership list of Luhman (2008) to be essentially complete down to $0.1\,M_\odot$.

2.1.2 Stellar density

The Cham I cluster comprises a northern and southern component with no obvious overall centre. For the northern component (centre $\alpha = 167.47°$, $\delta = -76.515°$) we determined a half-number radius of $0.85°$ or $2.37\,$pc at a distance of $160\,$pc (see Luhman 2008, for discussion) and $0.59°$ or $1.65\,$pc for the southern component (centre $167.06°$, $-77.567°$). This gives half-number radius densities of ~2 and ~5 stars/pc^3, respectively. Within radii of $0.25\,$pc and $0.10\,$pc the densities for the southern component are 275 ± 65 stars/pc^3 and 1190 ± 530 stars/pc^3 (with little difference for the northern component).

2.1.3 Stellar binarity

A number of studies have probed the binarity of this young cluster (e.g., Reipurth & Zinnecker 1993; Ghez et al. 1997), but here we make use of the Lafrenière et al. (2008) study which acquired adaptive optics imaging of more than 50% of the known population. Lafrenière et al. (2008) found 30 binary systems and 6 tertiary systems in a sample of 126 Cham I members with separations in the range 0.1–$6.0''$, corresponding to 16–960 au at a distance of 160 pc. They report a multiplicity fraction of $27\pm^{5}_{4}\%$ (CSF=$32\pm^{6}_{5}\%$) within this range, including only companions where the flux ratio is above their 90% completeness limits. Two apparent companions were discounted due to a low probability of being bound to the primary and follow-up spectroscopic observations which were inconsistent with the young age of the region (i.e., they were likely distant background stars).

2.2 IC 348

2.2.1 Membership

To estimate the stellar density in IC348, we have used the results of Luhman et al. (2003) who used optical and near-IR surveys, along with spectroscopic follow-up, to construct a census which is complete well into the substellar regime. For consistency, we have considered only those objects with spectral types of M6 or earlier, corresponding to sources above the substellar limit in this ~1–2 Myr old cluster. After removing the brown dwarfs, we are left with a stellar membership of 265 objects from the 288 known members.

2.2.2 Stellar density

Although subclustering is evident on spatial scales of ~0.1 pc (Lada & Lada 1995), IC348 shows a relatively symmetric radial profile. From a cluster centre of $56.160°,+32.166°$, we have determined a half-number radius of $303''$, or ~$0.464\,$pc at the cluster distance of $316\pm22\,$pc (Luhman et al. 2003; Strom et al. 1974), which gives a stellar density in excess of 300 stars/pc^3- a determination which is well-matched by those of Lada & Lada (1995) and Herbig (1998). Within radii of $0.25\,$pc and $0.10\,$pc, IC348 has stellar densities of 1115 ± 138 stars/pc^3 and 3819 ± 1111 stars/pc^3, respectively.

2.2.3 Stellar binarity

In the first binary survey of IC 348, Duchêne et al. (1999) reported the detection of 12 binary systems (and no higher order systems) from a sample of 66 targets systems using the survey of Herbig (1998) to define cluster membership. They were sensitive to binaries with separations down to $0.1''$, or ~32 au at a distance of 316 pc, and their maximum separation of $8.0''$ was chosen to restrict the confusion between real binary systems and background alignments. However, three apparent binaries were removed from the sample as they were identified as likely background stars due to their large separations and magnitude differences compared to the rest of the observed binary systems.

Duchêne et al. (1999) then use the known mass ratio distribution of the solar neighbourhood from Duquennoy & Mayor (1991) to estimate the number of undetected binary systems. They apply this small correction to determine the likely number of total binaries in IC348 and so derive a total multiplicity fraction of 19±5% (CSF=19±5%, since no $n > 2$ systems were found) within a separation range of 0.1–$8.0''$, or 32–2530 au at a distance of 316 pc. After accounting for stars rejected as non-members, but which appear in the more recent Luhman et al. (2003) compilation, we determined that the Duchêne et al. (1999) study detected 14 binaries from 71 targets systems, giving a multiplicity fraction of 20±5% over a separation range of 32–2530 au.

2.3 The ONC

2.3.1 Membership

Although a very well-studied region, there is no published list of confirmed stellar members down to the substellar limit which covers more than the centre of this rich star cluster. Therefore, to estimate the stellar density of the ONC, we have used the complementary membership lists of Hillenbrand (1997) (hereafter H97) and the *Chandra* Orion Ultradeep Project (COUP, Getman et al. 2005). The H97 observations cover a large area ($\sim0.5\times0.5^\circ$), but do not probe down to the substellar limit, while the COUP list is relatively complete to below $\sim0.1\,M_\odot$, but covers only the central $\sim17'\times17'$.

2.3.2 Stellar density

The ONC shows a slightly north-south elongated structure, but is centrally concentrated with a dense core. We therefore used the H97 list to determine a half-number radius of $390''$ centred on 83.8185°, -5.3875°, corresponding to $\sim0.78\,pc$ at a distance of $414\pm7\,pc$ (Menten et al. 2007). From this we extrapolate that the ONC has a stellar population of ~1700 stars and within the half-number radius has a stellar density of 425 ± 33 stars/pc^3. This increases to 4700 ± 290 stars/pc^3 within $0.25\,pc$ of the cluster centre and to $22,600\pm1200$ stars/pc^3 in the inner $0.1\,pc$.

2.3.3 Stellar binarity

There have been several studies of the binarity of stars in this nearby massive star-forming region. Prosser et al. (1994) reported an estimated *binary fraction* of $\sim11\%$ in the range 0.1–$1.0''$ (42–$420\,au$). Petr et al. (1998) then used high angular resolution near-IR imaging to probe ONC binaries and reported a *binary fraction* of $5.9\pm4.0\%$ in the separation range 0.14–$0.5''(58$–$207\,au)$, but they were hampered by very low numbers (only four binaries were detected).

   To provide the most comprehensive sample for comparison with other regions, we have chosen to use the more recent and wider-field HST survey of Reipurth et al. (2007) which imaged over 1000 stars, of which 781 have a high membership probability. They found 78 multiple systems with separations in the range 0.1–$1.5''$ (42–$620\,au$) and from the density of stars they estimated that 9 of their observed binaries were a result of projection effects. Reipurth et al. (2007) report a background-corrected multiplicity fraction of $8.5\%\pm1.0\%$ (CSF=$8.8\%\pm1.1\%$) in the range 0.15–$1.5''$, or 62–$620\,au$[1] This includes companions with flux ratios of up to $\Delta H\alpha\sim6^{\mathrm{m}}$.

2.4 Ophiuchus

2.4.1 Membership

Due to the large and dispersed nature of the ρ Ophiuchi complex we have chosen to focus on the main cloud, L1688. A census of the known members of this core was presented by Wilking et al. (2008) which they believe to be 'essentially complete' for class II and III objects. This is supported by their comparison of the X-ray luminosity functions of L1688 to that of the ONC from the deep COUP study of Feigelson et al. (2005). For consistency with the other regions studied here, we have used the Wilking et al. (2008) list of candidate brown dwarfs to remove those from the member list, leaving 295 known stellar members in L1688.

2.4.2 Stellar density

While the stellar density of the Ophiuchus association taken as a whole is relatively low, the density of the L1688 core is approximately an order of magnitude higher. The L1688 core shows significant sub-clustering with no obvious overdensity at the centre. Wilking et al. (2008) summarise the various distance estimates for the ρ Ophiuchus cloud (120–$145\,pc$) and so, similarly, we adopt a distance of $130\,pc$ to L1688. Using a cluster centre of 246.727°, -24.44°, we have determined a half-number radius of 0.234°, or $\sim0.5\,pc$ at the distance of L1688, which results in an mean density of 236 ± 27 stars/pc^3. Within radii of $0.25\,pc$ and $0.10\,pc$, L1688 has stellar densities of 611 ± 183 stars/pc^3 and 1910 ± 955 stars/pc^3, respectively.

2.4.3 Stellar binarity

In a lunar occultation and direct imaging search for binary stars, Simon et al. (1995) targeted 35 pre-main-sequence stars in Ophiuchus, but the small sample size frustrated their attempts to compare with surveys of Taurus. More recently, Ratzka et al. (2005) presented a binary survey of 158 young stellar systems in the ρ Ophiuchus molecular clouds, centred on the dark cloud L1688. They reported a multiplicity fraction of $29.1\pm4.3\%$ within a separation range of 0.13–$6.4''$ (corresponding to 17–$830\,au$ at $130\,pc$) where their observations were fully sensitive to flux ratios ≥0.1, but with a significant number of companions with higher flux ratios.

   However, if we consider only those systems which have been identified as members of Cham I in the recent Wilking et al. (2008) census, then we are left with 106 systems, of which 32 are binaries and 3 tertiary systems. Ratzka et al. (2005) also analysed the contribution of the background to the observed number of companions and determined that for their sample there should be three unidentified non-bound systems. Similarly, for our reduced sample, there should be two systems where the apparent companion is not bound, resulting in a multiplicity fraction of $31\pm6\%$ (CSF=$34\pm6\%$) within a separation range of 17–$830\,au$.

2.5 Taurus

2.5.1 Membership

A census of the known stellar and substellar pre-main sequence members of the Taurus-Auriga association was com-

---

[1] The separation range quoted here is different to that given by Reipurth et al. (2007) as we use the a newer distance from Menten et al. (2007), supported by Jeffries (2007) and Mayne & Naylor (2008).

piled by Kenyon et al. (2008) and updated by Luhman et al. (2009). The completeness of this sample was investigated by Luhman et al. (2009) who reported that the regions covered by the XEST survey (Güdel et al. 2007, where complimentary optical and IR surveys exist) are complete for class I and II stars and complete down to $0.02\,M_\odot$ for class II brown dwarfs. Deep, wide-field, optical, near-IR (Briceño et al. 2002; Luhman 2004; Guieu et al. 2006) and Spitzer imaging surveys (Luhman et al. 2010) of Taurus provide a high level of completeness into the substellar regime across the region. Therefore, to provide an essentially complete *stellar* membership list we have removed objects with spectral types later than M6, corresponding to sources above the substellar limit in this ~1–2 Myr old cluster, leaving 292 stars.

2.5.2 Stellar density

Due to the dispersed nature of the young stars in the ~1–2 Myr Taurus-Auriga association, it is not useful to define densities within a half number radius or within radii as small as 0.25 pc. We therefore report the average surface density of ~0.4±0.1 stars/pc^2 for the northern filament (defined here as $62°< \alpha < 72°$, $22°< \delta < 31°$) and the volume density of 6.0±1.2 stars/pc^3 within a radius of 1 pc from the centre of the densest core (L1495, centre 64.6°,+28.40°) using a distance of 140±14 pc (Wichmann et al. 1998; Köhler & Leinert 1998).

2.5.3 Stellar binarity

Although a number of authors have reported binary statistics for young stars in Taurus (Ghez et al. 1993; Duchêne et al. 2004), in some cases probing down to below 1 au (Simon et al. 1992, 1995), here we make use of the binary survey of Taurus presented by Leinert et al. (1993) which surveyed over 100 stellar members. We do not use the survey of Köhler & Leinert (1998) as the weak-lined T Tauri stars identified though their X-ray emission are more widespread across the region than the majority of the confirmed Taurus members, suggesting that they may be a separate population. That said, Köhler & Leinert (1998) find no significant difference in binarity between the weak-lined and classical T Tauri stars in the two samples. Leinert et al. (1993) reported a multiplicity fraction of 42±6% for their observations which were sensitive to systems with a flux ratio of up to $\Delta K = 2.5$ over a separation range of 0.13–13.0″, corresponding to 18–1820 au. The contribution of the background was examined and two apparent companions were discounted as their large separations and colours identified them as background stars. No other projected companions were expected in their sample.

If we consider only the targets within the area of the northern filament (as described above), Leinert et al. (1993) find 27 binary, 2 triple and 1 quadruple system from a total of 72 surveyed systems, giving a multiplicity fraction of 42±8% (CSF=47±8%) within a separation range of 18–1820 au.
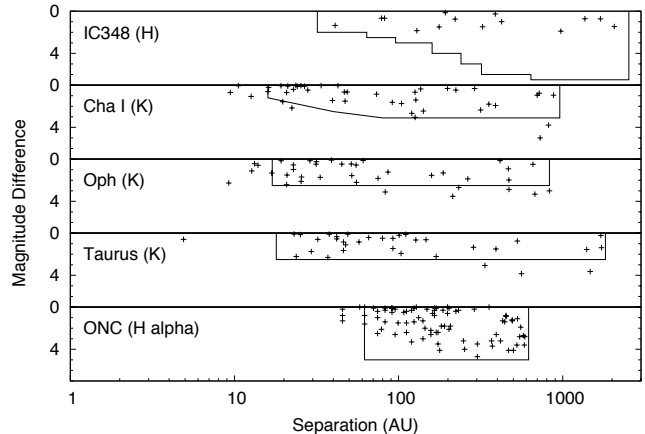
Figure 1. The contrast of each multiple system found in the five surveys shown as a function of separation. The filled lines demarcate the completeness of each survey. The labels identify the clusters and the filter used in the observations.

3 COMPARISON OF OBSERVED STELLAR BINARITY

3.1 Contrast sensitivities

To enable a fair comparison of the various binary surveys we must determine the contrast ratio to which each survey was sensitive. Table 2 lists the maximum contrast ratio for each survey in the passband employed while Fig. 1 shows how these vary with physical projected distance from the primary star. For simplicity, we aimed to use only surveys carried out in the K-band, but this was not possible for IC 348 and would have severely restricted the sample for the ONC, which used an H-band and the NICMOS F658N filter respectively. For the surveys carried out in the K-band, a common contrast cut of $\Delta K = 2.5$ was chosen.

To determine a conversion of the contrast in the H and F658N filters to the K-band, we have used the theoretical models of Siess et al. (2000). By considering primary stars at 1 Myr with masses in the range 0.1–3.0 $M_\odot$ and mass ratios of 0.1–1, we were able to predict the range of magnitude differences expected. Figure 2 shows the relation between model magnitude differences in the H and K-bands for this sample of possible systems. This clear linear relation allows us to convert our chosen common K-band contrast limit to an H-band contrast limit.

For the F658N filter, the situation is complicated by the lack of reported magnitudes in that filter for the theoretical models. However, comparisons with the IPHAS Hα, r' and Cousins R-band indicate that there is a near linear relation between magnitudes in these bands. We therefore compare the magnitude differences in the R and K bands to determine the appropriate contrast cut for the Reipurth et al. (2007) survey of the ONC. Figure 3 shows the relation between model magnitude differences in the R and K-bands for the primary masses and mass ratios described above. Although the structure observed does not provide such a clear correlation as for the H and K-bands, our ΔK limit of 2.5 allows most of this structure to be ignored and gives a contrast of F658N≃5. We also note that the majority of the Reipurth et al. (2007) binaries have contrasts of $\Delta R < 3.0$. This then
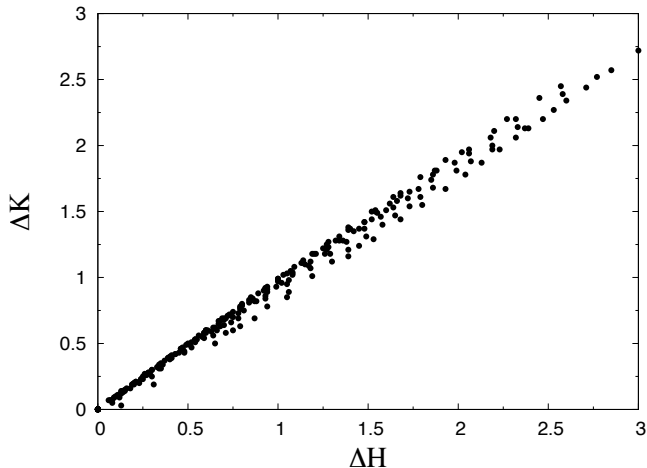
Figure 2. The magnitude difference in the H and K bands between primary and secondary stars using the predicted brightnesses from the 1 Myr Siess et al. (2000) evolutionary model for primary masses in the range 0.1–3.0 $M_\odot$ and mass ratios of 0.1–1.0.
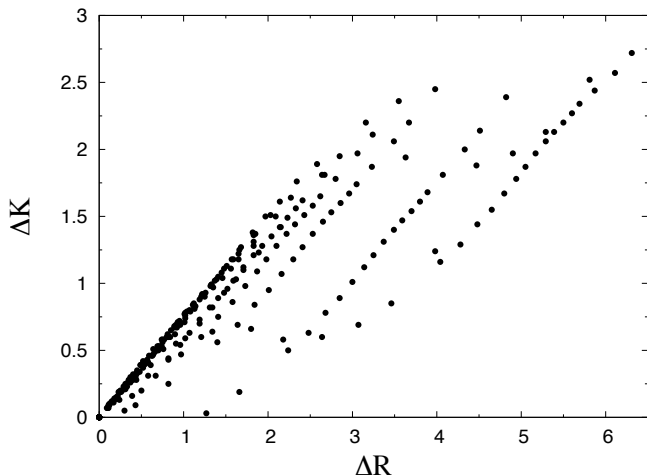
Figure 3. The magnitude difference in the R and K bands between primary and secondary stars using the predicted brightnesses from the 1 Myr Siess et al. (2000) evolutionary model for primary masses in the range 0.1–3.0 $M_\odot$ and mass ratios of 0.1–1.0.

allows us to apply a consistent contrast limit across the five surveys ($\Delta K = 2.5 => \Delta H = 2.7$, $\Delta F658N = 5$).

3.2   Primary mass and mass ratio

In the field the binarity of stars appears to decrease with primary mass (Duquennoy & Mayor 1991; Fischer & Marcy 1992; Lada 2006). Simulations suggest that dynamical destruction is relatively insensitive to primary mass (at least from M-dwarfs to G-dwarfs), and so this mass-dependence may reflect a primordial mass-binarity relationship (see Parker & Goodwin 2011). Therefore, in addition to matching contrast ratios between different surveys, we must ensure we cover the same masses of stars to avoid introducing a possible bias in the observed binarity. To do this we have used the spectral type reported in the various membership and
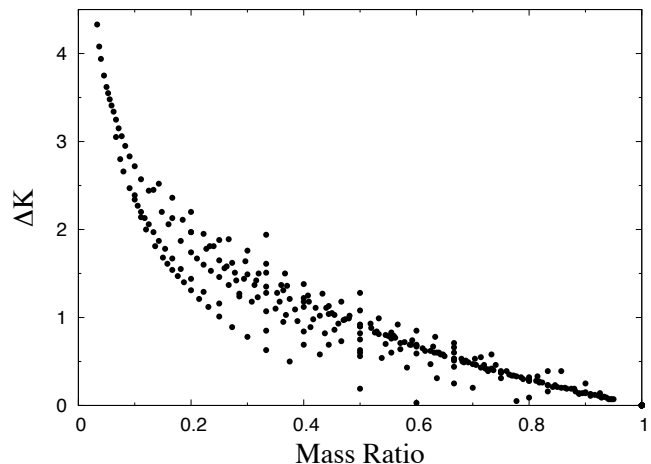
Figure 4. The K-band magnitude difference as a function of mass ratio for systems with primary and secondary masses in the range 0.1–3.0 $M_\odot$ from the 1 Myr Siess et al. (2000) evolutionary model.

binary survey papers for the survey targets to set upper and lower mass limits (Hillenbrand 1997; Lafrenière et al. 2008; Luhman & Rieke 1999; Luhman et al. 2003, 2009). Using the spectral type range of G5–M5.5 common to all five surveys, we have limited our comparison to primary stars with masses of ~0.1–3.0 $M_\odot$ assuming an age of 1 Myr (Siess et al. 2000).

While, for our survey comparison, we need not explicitly set limits on the range of mass ratios probed, we can use the theoretical models of Siess et al. (2000) to estimate the mass ratios given the contrast limit of $\Delta K = 2.5$. As shown in Fig. 4, the contrast limit we have adopted is approximately equivalent to a mass ratio of 0.1 for 0.1–3.0 $M_\odot$ primary stars at an age of ~1 Myr. We note however, that there will be a small bias due to differing levels of completeness in the binary surveys (assuming a variation with primary mass), i.e., one survey may have surveyed a larger fraction of lower mass stars than another and so may find a slightly decreased binarity.

3.3   Separation sensitivities

The final cuts necessary to compare the binary surveys are to the separation ranges probed. As the ONC is the farthest and densest of our regions, it sets a limit on the upper and lower separation probed by all five surveys. However, applying this to all five surveys would severely restrict the number of binary systems. We therefore present a comparison of the five surveys with three different separation range cuts. Cut 1 (18–830 au) allows us to compare the widest possible separation range for Cham I, Ophiuchus and Taurus; cut 2 (32–830 au) also includes IC 348; and cut 3 (62–620 au) allows a comparison of all five regions.

4   OBSERVATIONAL RESULTS

In Table 3 we show the comparable multiplicity fractions for the five regions in the three separation ranges. For each region the companions and targets of the binary surveys have
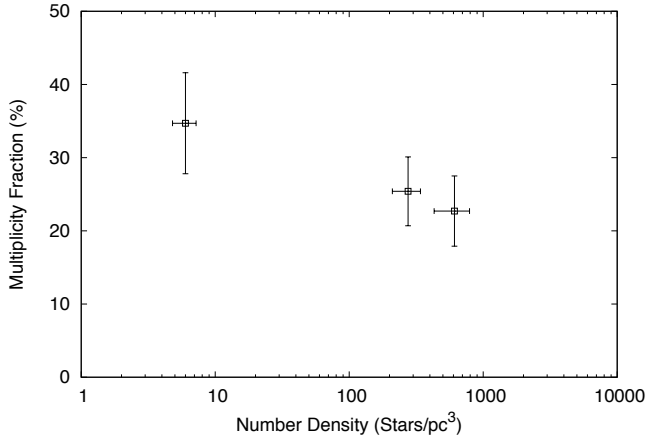
Figure 5. The stellar multiplicity fractions of Taurus, Cham I and Ophiuchus against stellar density when we consider the same contrast cuts, stellar masses and a separation range of 18–830 au. The densities are calculated within a projected distance of 0.25 pc from the cluster centre, except in the case of Taurus where a radius of 1 pc is used.

been removed where the spectral types are not within the range G5–M5.5 and where the magnitude difference exceeds 2.5^{m}. In the case of the ONC, the spectral type information was not available so no mass cuts have been made to the sample. This is likely to mean the binarity is higher than it should be for this comparison due to the (postulated) increasing binarity with stellar mass (see, e.g., Raghavan et al. 2010; Parker & Goodwin 2011).

For comparison, a log-normal field G-dwarf-like distribution ($\mu_{\log a} = 1.57$, $\sigma_{\log a} = 1.53$, with a 60 per cent *total* binary fraction) would have a binary fraction of 24 per cent in the range $18-830$ au, 20 per cent in the range $32-830$ au, and 14 per cent in the range $62-620$ au. Similarly, for an M-dwarf-like distribution with a *total* binary fraction of 40 per cent (and the same log-normal parameters) the binary fractions would be 16, 13, and 9 per cent respectively. As most stars in our samples are M-dwarfs the most reasonable comparison is to the M-dwarf-like field distribution.

In the $18-830$ au range all clusters are over-abundant in binaries compared to the M-dwarf-like field distribution, and Taurus very significantly so. In the $32 - 830$ au range only Taurus and Cham I are over-abundant, and in the $62-620$ au range only Taurus has a significant excess. We will return to this in the discussion.

4.1 Binarity variations with stellar density

Given that binary fractions are thought to evolve due to the dynamical destruction of binaries it is usually assumed that there should be a decrease in the binary fraction with stellar density (Kroupa 1995a,b; Parker et al. 2009). This relationship is thought to be seen in the significant differences in the binary fractions of Taurus and the ONC (~ 17 per cent versus ~ 8.5 per cent respectively).

In Figs. 5 and 6 we show the binary fractions against density for the range 18–820 au (for Taurus, Cham I, and Ophiuchus), and 62–620 au (for all five clusters). In all cases the density is calculated within a projected radius of 0.25 pc, except Taurus which is within a 1 pc projected radius.
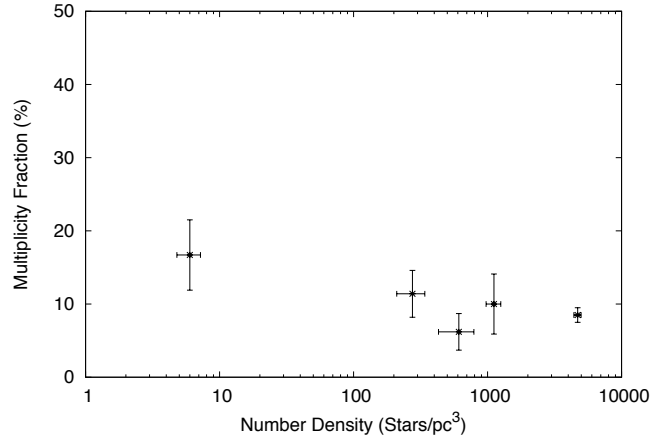
Figure 6. The stellar multiplicity fractions of all five regions against stellar density when we consider the same contrast cuts, stellar masses and a separation range of 62–620 au. The densities are calculated as for Fig. 5.

Table 3. Stellar densities and multiplicity fractions for the three separation ranges.

| Region	Stellar Density (star pc^{-3})	Multiplicity fraction (per cent)
Separation = 18–830 au		
Taurus	6.0 ± 1.2	34.7 ± 6.9
Cham I	275 ± 65	25.4 ± 4.7
Ophiuchus/L1688	610 ± 180	22.7 ± 4.8
Separation = 32–830 au		
Taurus	6.0 ± 1.2	29.2 ± 6.4
Cham I	275 ± 65	17.5 ± 3.9
Ophiuchus/L1688	610 ± 180	14.4 ± 3.9
IC 348	1115 ± 140	11.7 ± 4.4
Separation = 62–620 au		
Taurus	6.0 ± 1.2	16.7 ± 4.8
Cham I	275 ± 65	11.4 ± 3.2
Ophiuchus/L1688	610 ± 180	6.2 ± 2.5
IC 348	1115 ± 140	10.0 ± 4.1
ONC	4700 ± 290	8.5 ± 1.0

There is a relationship between binary fraction and density, but this relationship is driven almost entirely by Taurus. In Fig. 6 in particular, the relationship without Taurus is weak at best. This is rather unexpected as the four clusters (without Taurus) span more than a decade in density.

4.2 Observed morphologies

We have used the stellar density of clusters detailed above, but there are problems associated with the determination (or meaning) of an average density in at least two of our clusters (Taurus and Cham I). In smooth distributions taking a typical stellar density as a measure of the proximity of stars and the likelihood of encounters is perfectly reasonable. However, at least two of the clusters we are examining are far from smooth and it is questionable to what extent a 'stellar density' is a meaningful concept.
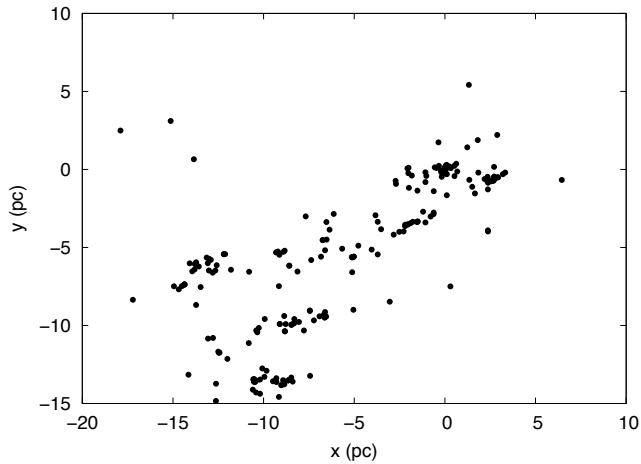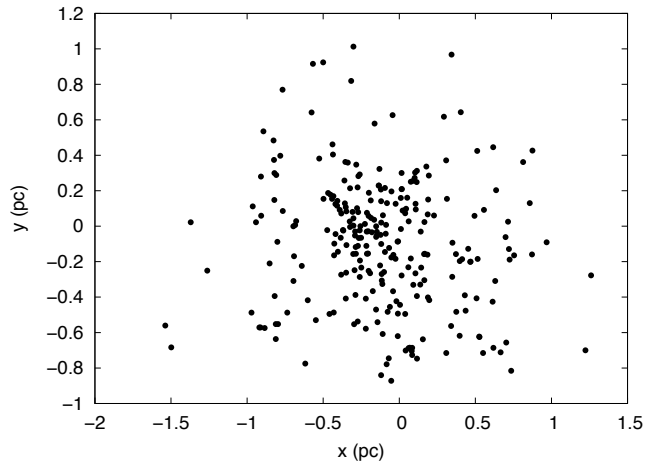
Figure 7. The locations of each of the members of the northern filament of the Taurus Molecular Cloud (as described in Sect. 2) with physical projected separations assuming a distance of 140 pc.
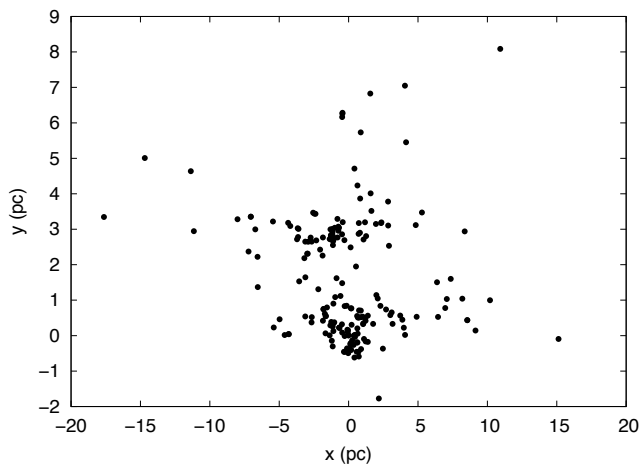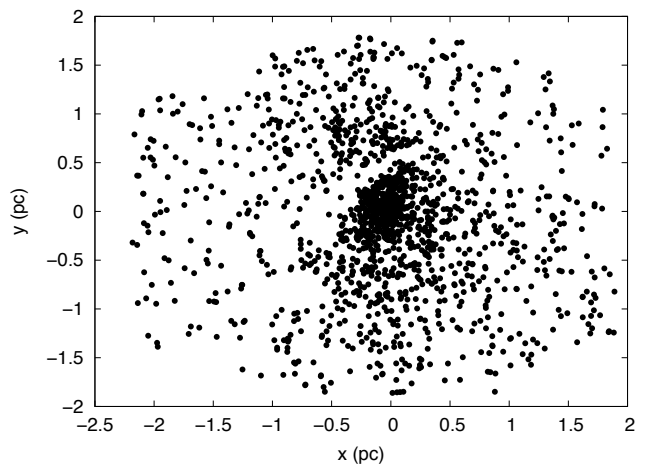

Figure 8. The locations of each of the members of the Cham I cluster with physical projected separations assuming a distance of 160 pc.
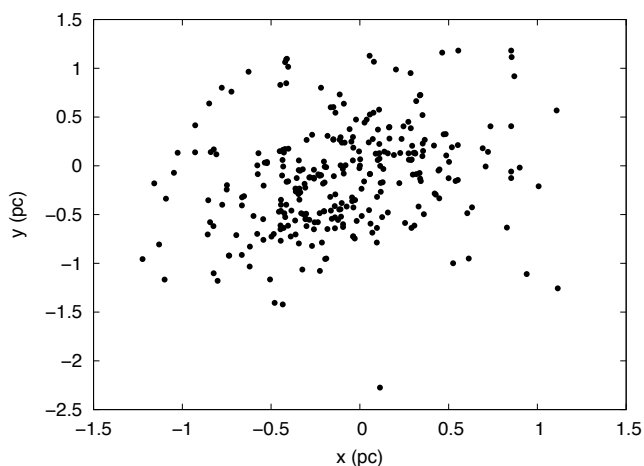
Figure 9. The locations of each of the members of the L1688 core in Ophiuchus with physical projected separations assuming a distance of 130 pc.

Figure 10. The locations of each of the members of IC348 with physical projected separations assuming a distance of 316 pc.

Figure 11. The locations of each of the members of the Orion Nebula Cluster from Hillenbrand (1997) with physical projected separations assuming a distance of 414 pc. These observations clearly miss some of the cluster members farthest from the centre and do not extend down to the stellar/substellar limit (see Sect. 2.3). The absorption feature associated with the 'lip' of the emission nebula is seen as an under-density of sources in a strip across the map (see Hillenbrand 1997).

In Figs. 7 to 11 we show the (two-dimensional) stellar distributions in each of our regions. Ophiuchus, IC348 and the ONC (Figs. 9, 10, and 11) are fair examples of classic 'clusters': centrally concentrated with density declining with radius. However, Taurus and Cham I (Figs. 7 and 8) are clearly very sub-structured and far from smooth. Despite our earlier attempt to define a 'stellar density', it is very unclear from these figures if a global 'density' has any meaning whatsoever. We address this question in the next section and in the discussion.

5   SIMULATIONS OF BINARY DESTRUCTION

In this section we attempt to use the observations of the cluster morphologies and multiplicity fractions to construct *N*-body models of star clusters to 'reverse engineer' the current

state to determine the primordial binary fractions (Kroupa 1995b).

It is well-known that many binaries are destroyed in dense environments (Heggie 1975; Hills 1975), and much theoretical work has gone into modelling the evolution of stellar binary properties in different clustered environments. The first comprehensive simulations were performed by Kroupa (1995a,b,c), who showed that a primordial binary separation distribution similar to that observed in Taurus–Auriga (Leinert et al. 1993) can evolve into a field-like (Duquennoy & Mayor 1991) separation distribution if the cluster is dense enough.

Kroupa (1995a,b) and Kroupa & Petr-Gotzens (2011) derive a *universal* pre-main sequence separation distribution based on these simulations, which is characterised by an initial binary fraction and an excess of binaries with separations $a > 10^3$ au, compared to the Galactic field. Recently, Marks, Kroupa & Oh (2011) have developed an analytical operator, which, depending on the cluster's initial density, can be used to predict the effects of dynamical evolution on the binary separation distribution in any star forming environment, if the primordial binary population is described by the (Kroupa 1995a) distribution. This operator assumes that the cluster is roughly spherical and relaxed at birth.

However, the assumption that clusters are roughly spherical and relaxed at birth is almost certainly not a reasonable assumption (see the distributions of Taurus and Cham I in Figs. 7 and 8 above). Also, although L1688 (Oph), IC348 and the ONC appear fairly smooth now, they may well have formed in a clumpy, complex distribution with their current smooth appearance due to dynamical evolution (see Allison et al. 2009, 2010; Parker et al. 2011). Parker et al. (2011) show that there can be significant binary processing even in low-density clusters if they are initially substructured. This is because the *local* density can be high enough to destroy binaries even if the average global density is very low. After a crossing time the initial substructure is erased and the cluster is roughly spherical and relaxed. Therefore two clusters that are almost identical at 1–2 Myr old can have a very different past dynamical history and therefore very different processing of their initial binary populations.

In this section we will simulate the evolution of clusters starting from clumpy and smooth initial distributions with sizes and densities chosen to roughly match our five observed clusters. We model the initial binary populations in the simulations as a Duquennoy & Mayor-like wide lognormal with either a 45, 73 or 100 per cent initial binary fraction.

5.1   Cluster membership

In order to match the observed clusters as closely as possible, we use approximately the same numbers of stars in our simulations of each cluster as are observed. Therefore, our clusters designed to mimic Cham I contain 200 stars, IC348-like clusters contain 260 stars, the ONC-like clusters contain 1500 stars; and the Ophiuchus- and Taurus-like clusters contain 300 stars.

We keep the number of stars fixed; however, for different primordial binary fractions this results in different numbers of systems. For example, a Taurus-like cluster with 300 stars

and a primordial binary fraction of 100 per cent contains 150 stellar systems, all of which are binaries; a similar cluster with a field-like binary fraction ($\sim$ 45 per cent) contains 200 systems, 100 of which are binaries. We note that this may underestimate the number of stars in each cluster, as binary systems outside of the observable separation ranges would be either unresolved or seen as two independent stars.

5.2   Stellar systems

To create a stellar system, the mass of the primary star is chosen randomly from a Kroupa (2002) IMF of the form

$$N(M) \propto \left\{ \begin{array}{ll} M^{-1.3} & m_0 < M/\mathrm{M}_\odot \leq m_1\,, \\ M^{-2.3} & m_1 < M/\mathrm{M}_\odot \leq m_2\,, \end{array} \right. \tag{3}$$

where $m_0 = 0.1\,\mathrm{M}_\odot$, $m_1 = 0.5\,\mathrm{M}_\odot$, and $m_2 = 50\,\mathrm{M}_\odot$. We do not include brown dwarfs in the simulations as these have been removed from the observational samples.

We then assign a secondary component to the system depending on the binary fraction associated with the primary mass: field-like, 73 per cent, and 100 per cent.

For a field-like binary fraction we divide primaries into four groups. Primary masses in the range $0.1 \leq m_p/\mathrm{M}_\odot < 0.47$ are M-dwarfs, with a binary fraction of 0.42 (Fischer & Marcy 1992). K-dwarfs have masses in the range $0.47 \leq m_p/\mathrm{M}_\odot < 0.84$ with a binary fraction of 0.45 (Mayor et al. 1992), and G-dwarfs have masses from $0.84 \leq m_p/\mathrm{M}_\odot < 1.2$ with a binary fraction of 0.57 (Duquennoy & Mayor 1991; Raghavan et al. 2010). All stars more massive than $1.2\,\mathrm{M}_\odot$ are grouped together and assigned a binary fraction of unity, as massive stars have a much larger binary fraction than low-mass stars (e.g. Abt et al. 1990; Mason et al. 1998; Kouwenhoven et al. 2005, 2007; Pfalzner & Olczak 2007; Mason et al. 2009, and references therein).

For the 100 per cent binary fractions *all* stars are in binaries. For the 73 per cent binary fractions, 73 per cent of all stars (regardless of mass) are in binary systems. This sounds like a rather arbitrary number, but as we will describe below it is this binary fraction that provides the best fit to all of the clusters.

Secondary masses are drawn from a flat mass ratio distribution; recent work by Reggiani & Meyer (2011) has shown the mass ratio of field binaries to be consistent with being drawn from a flat distribution, rather than random pairing from the IMF.

We draw the periods of the binary systems from the $\log_{10}$-normal fit to the G-dwarfs in the field by Duquennoy & Mayor (1991) – see also Raghavan et al. (2010), which has also been extrapolated to fit the period distributions of the K- and M-dwarfs (Mayor et al. 1992; Fischer & Marcy 1992):

$$f\left(\log_{10}P\right) \propto \exp\left\{ \frac{-(\log_{10}P - \overline{\log_{10}P})^2}{2\sigma_{\log_{10}P}^2} \right\}, \tag{4}$$

where $\overline{\log_{10}P} = 4.8$, $\sigma_{\log_{10}P} = 2.3$ and P is in days. We convert the periods to semi-major axes using the masses of the binary components.

The eccentricities of binary stars are drawn from a thermal distribution (Heggie 1975; Kroupa 2008) of the form

$$f_e(e) = 2e. \tag{5}$$

In the sample of Duquennoy & Mayor (1991), close binaries (with periods less than 10 days) are almost exclusively on tidally circularised orbits. We account for this by reselecting the eccentricity of a system if it exceeds the following period-dependent value (Parker & Goodwin 2011):

$$e_{\rm tid} = \frac{1}{2} \left[0.95 + \tanh \left(0.6 \log_{10} P - 1.7 \right) \right]. \qquad (6)$$

We combine the primary and secondary masses of the binaries with their semi-major axes and eccentricities to determine the relative velocity and radial components of the stars in each system. The binaries are then placed at the centre of mass and velocity for each system in a fractal or Plummer sphere (see below).

5.3   Numerical parameters

The simulations are run for 10 Myr using the `kira` integrator in the Starlab package (e.g. Portegies Zwart et al. 1999, 2001) and the binary fractions and densities are determined after 1 Myr. We do not include stellar evolution in the simulations. As no systems of higher order than $n = 2$ form, the binary fraction is equivalent to the multiplicity fraction. Details of each simulation are presented in Table 4.

We determine whether a star is in a bound binary system using the nearest neighbour algorithm outlined in Parker et al. (2009) and Kouwenhoven et al. (2010). If two stars are closer than the average local stellar separation, are also mutual nearest neighbours, and have a negative binding energy, then they are in a bound binary system.

In principle, this differs from an observer's definition of a visual binary, which could include chance associations along the line of sight. However, numerical experiments indicate that the total number that could merely be chance associations is negligible.

5.4   'Observing' simulations

We analyse the binary fractions of clusters in a way as close as possible to the observations. We only 'observe' binaries in the separation ranges matched by the real observations, taking closer binaries to be single unresolved stars, and wider binaries to be two separate stars. We only 'observe' systems with primary masses in the range $0.1\,{\rm M}_\odot \leq m_p < 3.0\,{\rm M}_\odot$, and with mass ratios $q = m_s/m_p \geq 0.1$.

To determine the stellar densities of the clusters we use the same method as applied to the real clusters, determining the volume densities within 0.25 pc from a 2D centroid fit to the centre of the cluster for our models for the ONC-, Ophiuchus- and IC348-like clusters. As with the observations, such a determination is problematic for sub-structured distributions, but we use it in the absence of anything better.

For our Cham I-like and Taurus-like clusters, we measure the stellar surface density for each star, according to the prescription of Casertano & Hut (1985):

$$\Sigma = \frac{N-1}{\pi D_N^2}, \qquad (7)$$

where N is the $N^{\rm th}$ nearest neighbour (we choose $N = 7$) and D_N is the projected distance to that nearest neighbour. We then determine the star with the highest surface density

and measure the volume density from that star, adopting a radius of 0.25 pc for Cham I and 1 pc for Taurus.

5.5   Cluster set-up and morphologies

We assume two different morphologies for the initial conditions of our clusters. Firstly, we model clusters as radially smooth Plummer spheres (Plummer 1911), which are used extensively in modelling the dynamical evolution of star clusters (e.g. Kroupa et al. 1999; Moraux et al. 2007; Parker et al. 2009). Secondly, we adopt a fractal distribution so that our clusters contain substructure initially (e.g. Goodwin & Whitworth 2004; Allison et al. 2010; Parker et al. 2011). In two dimensions these model set-ups reproduce, to first order, the entire range of observed morphologies described in Section 5, although we note that other set-ups, such as the King profile (e.g. King 1966) can, and have been used to fit several of the observed clusters (e.g. the ONC Hillenbrand & Hartmann 1998).

Our aim is to produce clusters that have the same morphology, density, and binary fractions as the observed clusters at the age of the observed clusters.
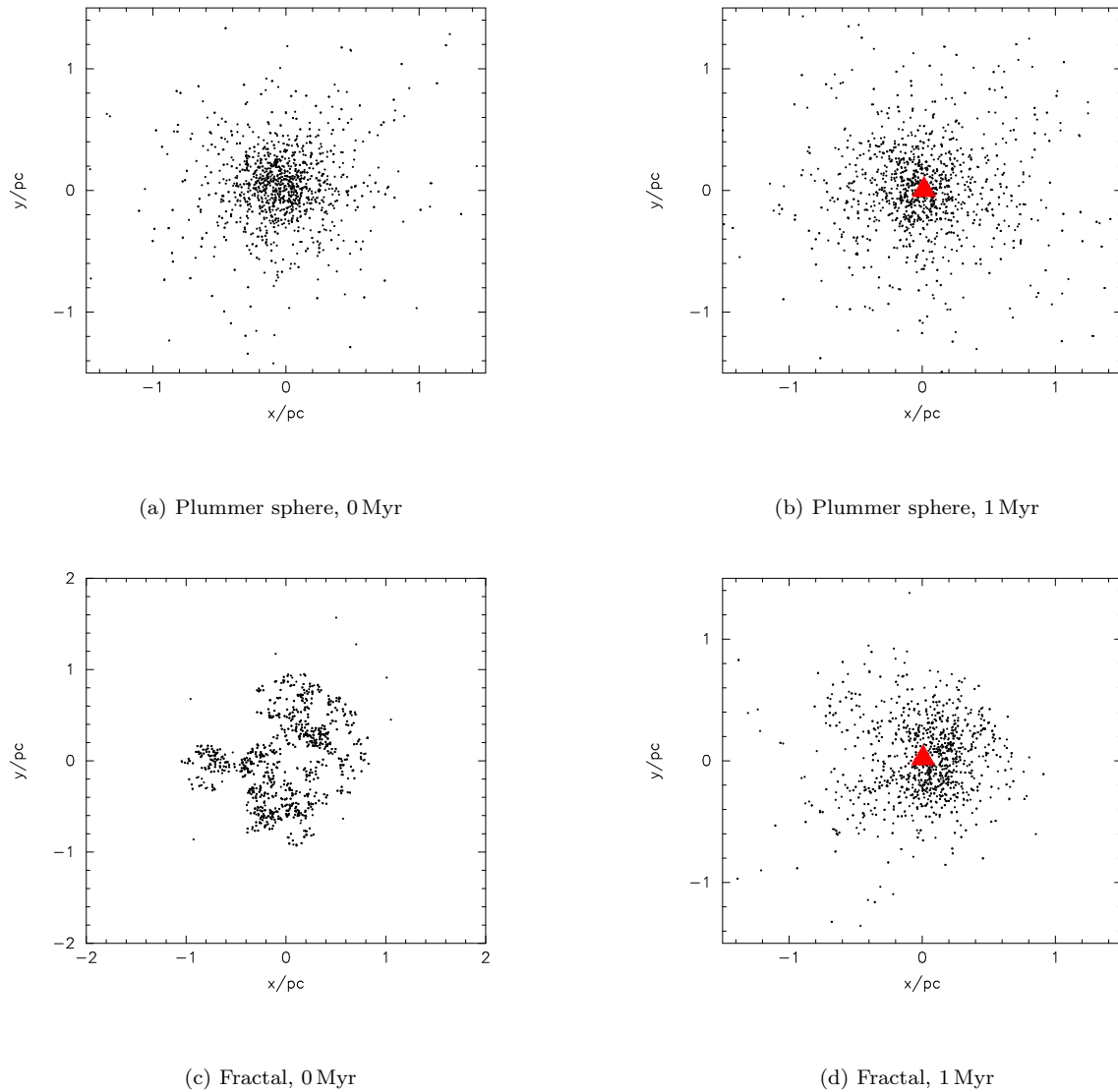
5.5.1   Plummer spheres

Plummer spheres (and fractals, see below) are used as initial conditions for the clusters that are observed to be roughly spherical, namely the ONC, Ophiuchus and IC348. Due to their obviously substructured nature we do not attempt to model Cham I or Taurus with Plummer spheres as initial conditions. We set up Plummer spheres according to the prescription in Aarseth, Henon & Wielen (1974), and we assume that they are in virial equilibrium at the start of the simulations.

We assume three different half-mass radii for the simulated clusters; 0.1, 0.4 and 0.8 pc. For an ONC-like cluster, a half-mass radius of 0.1 pc corresponds to an initial density of $\sim 10^4\,{\rm M}_\odot{\rm pc}^{-3}$, which is significantly higher than the observed value. However, Parker et al. (2009) show that such a cluster expands during the first 1 Myr of evolution and may have a similar density to the ONC after this time. A half-mass radius of 0.8 pc corresponds to the half-mass radius of the ONC today (Hillenbrand & Hartmann 1998).

We show examples of Plummer sphere morphologies for simulations of three of the observed clusters (details of the cluster set-up are given in Table 4). In Fig. 12 we show a Plummer sphere with 1500 stars, and a half-mass radius[2] of 0.4 pc (simulation ID = 2 in Table 4, before dynamical evolution (Fig. 12(a)) and at 1 Myr (Fig. 12(b)). This corresponds to an ONC-like cluster, if the cluster formed without substructure.

We also show Plummer sphere morphologies for our IC348- and Ophiuchus-like clusters. In Fig. 13 we show a Plummer sphere with 260 stars, and a half-mass radius of 0.4 pc (IC348, simulation ID = 7 in Table 4), and in Fig. 14 we show a Plummer sphere with 300 stars, and a half-mass radius of 0.8 pc (Ophiuchus, simulation ID = 13 in Table 4).

---

[2] We assume that there is no primordial mass segregation, so this also corresponds to the half-number radius.

(a) Plummer sphere, 0 Myr

(b) Plummer sphere, 1 Myr

(c) Fractal, 0 Myr

(d) Fractal, 1 Myr

Figure 12. Typical morphologies for our different initial conditions for ONC-like clusters. In the top panels we show a Plummer sphere with an initial half-mass radius of 0.4 pc at (a) 0 Myr and (b) 1 Myr. In the bottom panels we show a collapsing fractal cluster at (c) 0 Myr and (d) 1 Myr. The centroid position in the cluster at 1 Myr is marked in panels (b) and (d) by the red triangle.

In both figures, panel (a) shows the cluster before dynamical evolution, and panel (b) shows the cluster at 1 Myr.

All the Plummer sphere clusters are in virial equilibrium ($Q = 0.5$, where $Q = T/|\Omega|$, and T and Ω are the total kinetic energy and total potential energy of the stars) at the start of the simulations.

5.5.2 Fractals

Observations of young star forming regions show that a large amount of substructure is present in young star-forming regions (e.g. Sánchez & Alfaro 2010; Schmeja 2011). We employ a relatively straightforward way of modelling substructure using a fractal (see e.g., Goodwin & Whitworth 2004). In a fractal, the level of substructure is set by just one number, the fractal dimension D. A highly sub-structured clus-

ter has $D = 1.6$, whereas a cluster with no substructure has $D = 3.0$. For the ONC-like clusters we adopt $D = 2.0$ (a moderate amount of substructure), whereas the Cham I- and Taurus-like clusters have $D = 1.6$.

We refer the interested reader to Goodwin & Whitworth (2004); Allison et al. (2010); Parker et al. (2011) for a full description of the fractal set-up. Here, we briefly summarise the main features of the model. A cube is constructed, at the centre of which a 'parent' is placed. This then spawns subcubes, each of which contains a child at its centre. The fractal is built by determining how many of the children become parents, which is governed by the fractal dimension, D. For a lower fractal dimension, fewer children survive, and the cluster contains more substructure. The cube is pruned to make a sphere, and then children are randomly removed until the required number of 'stars' remain.

(a) Plummer sphere, 0 Myr

(b) Plummer sphere, 1 Myr

(c) Fractal, 0 Myr

(d) Fractal, 1 Myr
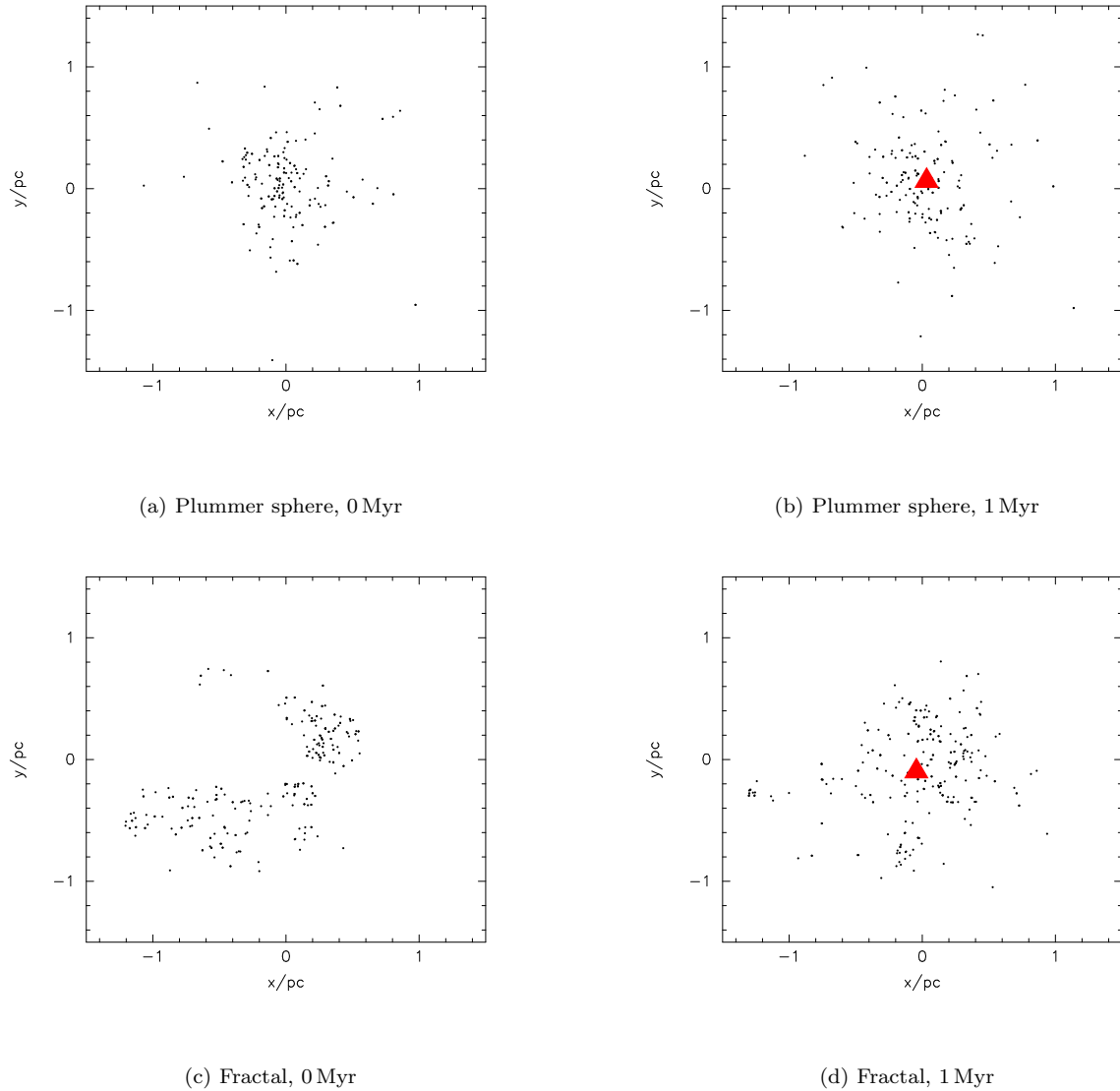
Figure 13. Typical morphologies for our different initial conditions for IC348-like clusters. In the top panels we show a Plummer sphere with an initial half-mass radius of 0.4 pc at (a) 0 Myr and (b) 1 Myr. In the bottom panels we show a collapsing fractal cluster at (c) 0 Myr and (d) 1 Myr. The centroid position in the cluster at 1 Myr is marked in panels (b) and (d) by the red triangle.

The velocities of stars in the fractal are determined thus; first generation children are assigned velocities from a Gaussian of mean zero, and children inherit their parent's velocity plus a random component that decreases with each generation in the fractal. This results in a velocity structure where nearby stars have very similar velocities, but distant stars can have very different velocities. The velocity of every star is then scaled to obtain the desired virial ratio of the cluster.

We set up some fractal clusters in virial equilibrium ($Q = 0.5$), and others are sub-virial (cool, $Q = 0.3$). Allison et al. (2010) have shown that a $N = 1000$ fractal with an initial size of 1 pc, and sub-virial velocities, will collapse and reach a very dense phase after ~1 Myr. This model has been successful in matching the observed levels of mass segregation in the ONC through dynamics (Allison et al. 2009), forming Trapezium-like systems (Allison & Goodwin 2011),

and dynamically processing binaries (Parker et al. 2011). However, it is unclear whether lower-mass clusters can also undergo this cool collapse phase within 1 Myr.

We show typical examples of the fractal morphologies for all of our simulated clusters. We model the ONC with a fractal of radius ~ 1 pc, an initial virial ratio of $Q = 0.3$ and a fractal dimension $D = 2.0$. In Fig. 12 we show the fractal model for the ONC (simulation ID = 4 in Table 4) before dynamical evolution (panel(c)) and after 1 Myr (panel(d)).

A key point to note in Fig. 12 is that the Plummer sphere and fractal initial conditions look very different at 0 Myr, but by 1 Myr the fractal has relaxed and the two clusters appear very similar (the initially fractal cluster is slightly more compact). The ONC fractal cluster models assume that the cluster is sub-virial (cool), which causes the

(a) Plummer sphere, 0 Myr

(b) Plummer sphere, 1 Myr

(c) Fractal, 0 Myr

(d) Fractal, 1 Myr
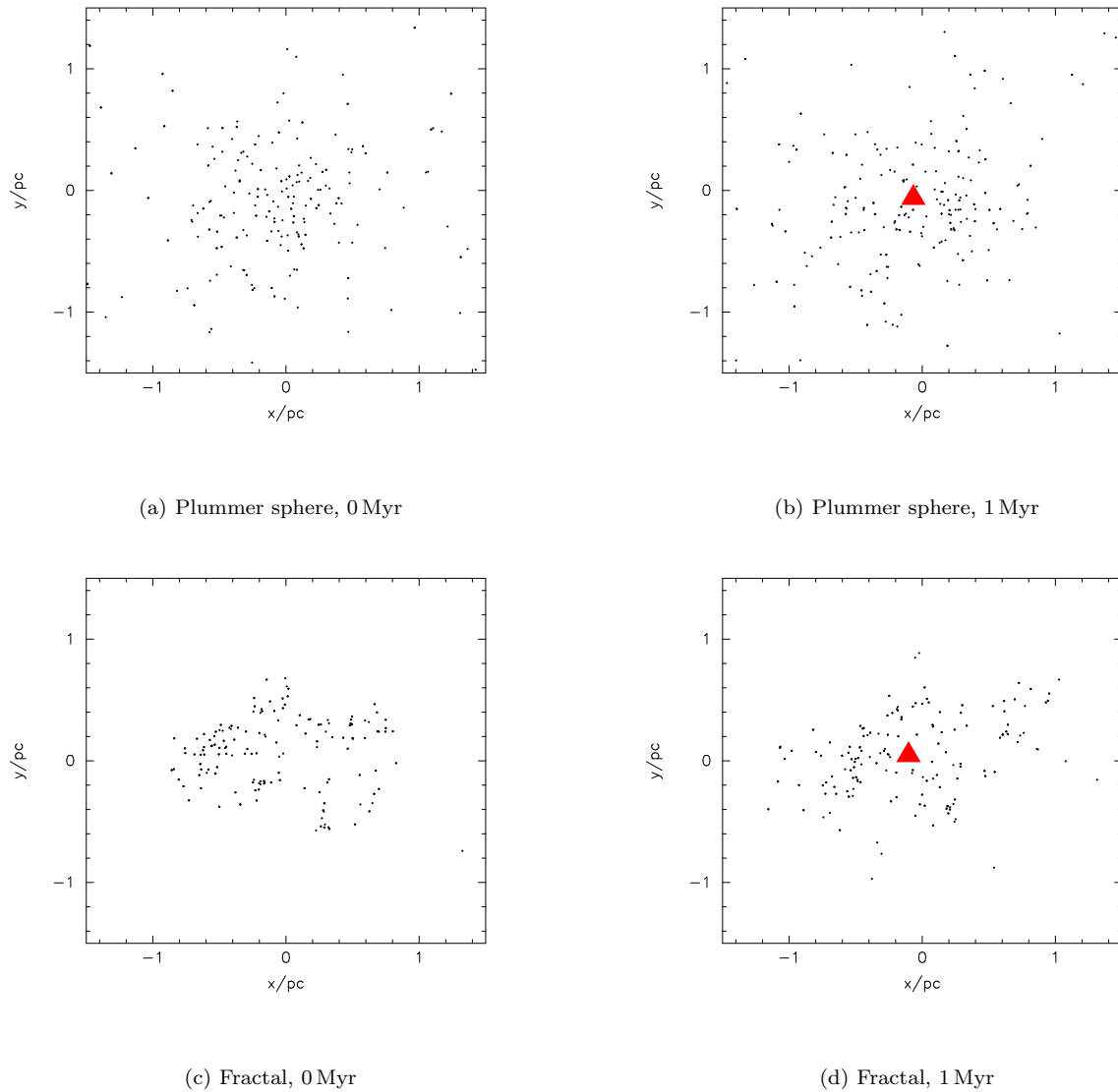
Figure 14. Typical morphologies for our different initial conditions for Ophiuchus-like clusters. In the top panels we show a Plummer sphere with an initial half-mass radius of 0.8 pc at (a) 0 Myr and (b) 1 Myr. In the bottom panels we show a fractal cluster in virial equilibrium at (c) 0 Myr and (d) 1 Myr. The centroid position in the cluster at 1 Myr is marked in panels (b) and (d) by the red triangle.

cluster to undergo a collapse, forming a dense core (see Allison et al. (2010) for details).

As the central density of IC348 is 1115 ± 140 stars pc^3, significantly higher than most star forming regions (e.g. Bressert et al. 2010), we test whether this cluster also underwent a cool collapse phase. We also model IC348 with a fractal of radius ~ 1 pc, an initial virial ratio of $Q = 0.3$ and a fractal dimension $D = 2.0$ (simulation ID = 10 in Table 4), and typical morphologies are shown in Fig. 13. The cluster before dynamical evolution is shown in Fig. 13(c) and at 1 Myr in Fig. 13(d), with the centroid of the cluster shown by the red cross.

In contrast to IC348, Ophiuchus is relatively sparse, with a central density of 610 ± 180 stars pc^3. We elect to model this cluster as a fractal in virial equilibrium ($Q = 0.5$); even if this cluster is undergoing cool collapse, it will not

reach its densest phase until long after 1 Myr. However, the map of the cluster (Fig. 9) shows a moderate level of substructure in this cluster. We therefore set up the cluster with fractal dimension $D = 2.0$ and a radius of ~ 1 pc (simulation ID = 14 in Table 4), and with typical morphologies as shown in Fig. 14. The cluster before dynamical evolution is shown in Fig. 14(c) and at 1 Myr in Fig. 14(d), with the centroid of the cluster shown by a red cross.

The Cham I cluster appears to be highly sub-structured and relatively sparse (recall Fig. 8). If clusters form with large amounts of sub-structure, which is then subsequently erased by dynamics, then we can already hypothesise that this cluster has not undergone much dynamical evolution. We model this cluster as a highly sub-structured fractal ($D = 1.6$) with radius 3 pc, in virial equilibrium $Q = 0.5$ (simulation ID = 16 in Table 4), and with typical morphologies

(a) Fractal, 0 Myr

(b) Fractal, 1 Myr
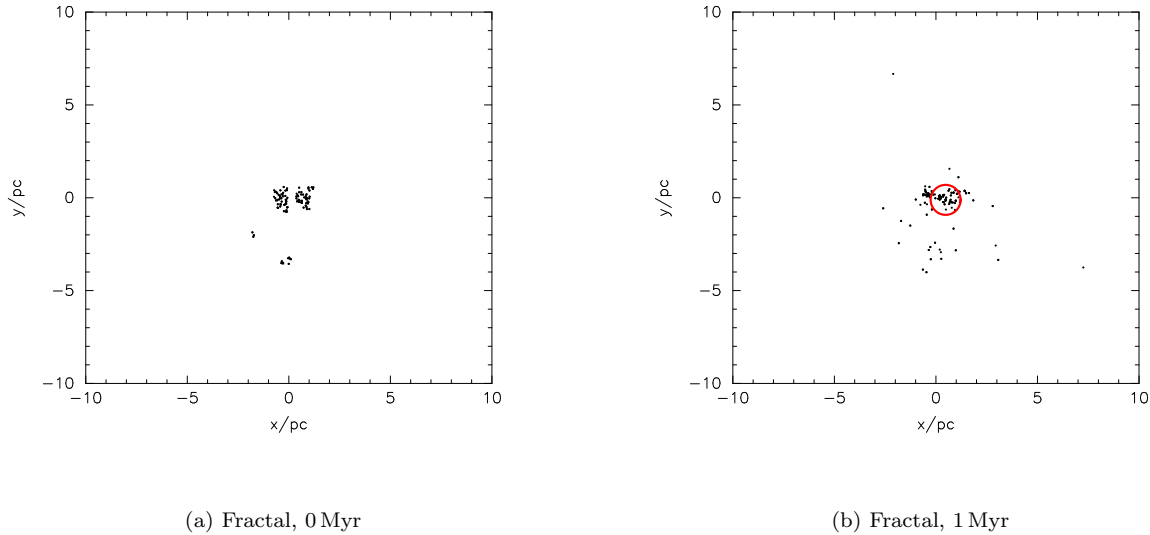
Figure 15. Typical morphologies for Chamaeleon-like clusters. We show a fractal in virial equilibrium at (a) 0 Myr and (b) 1 Myr. We show the star with the maximum local surface density (the point from which we measure the stellar density) at 1 Myr by a red circle.

(a) Fractal, 0 Myr

(b) Fractal, 1 Myr
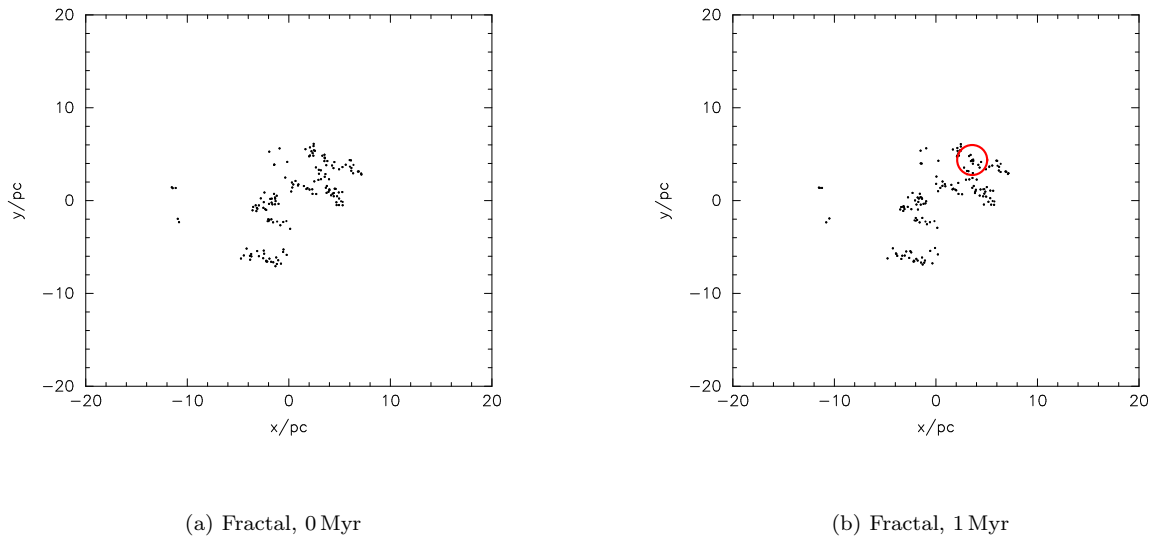
Figure 16. Typical morphologies for Taurus-like clusters. We show a fractal in virial equilibrium at (a) 0 Myr and (b) 1 Myr. We show the star with the maximum local surface density (the point from which we measure the stellar density) at 1 Myr by a red circle.

as shown in Fig. 15. The cluster before dynamical evolution is shown in Fig. 15(a) and at 1 Myr in Fig. 15(b). As there is no well-defined centre of the cluster, we mark the location in the cluster with the highest stellar surface density with a red circle.

Similarly, Taurus is also highly sub-structured, without a well defined centre. We model this cluster as a highly sub-structured fractal ($D = 1.6$) with radius 10 pc, in virial equilibrium $Q = 0.5$ (simulation ID $= 18$ in Table 4), and with typical morphologies as shown in Fig. 16. The cluster before dynamical evolution is shown in Fig. 16(a) and at 1 Myr in Fig. 16(b). Again, as there is no well-defined centre

of the cluster, we mark the location in the cluster with the highest stellar surface density by a red circle.

5.6   Results

Our ensembles of simulations with the symbols used in Figs. 17–22 are summarised in Table. 4. In the figures we show the multiplicity after 1 Myr in the applicable separation ranges for each ensemble of simulations against the stellar number density and the observed values for each cluster as the red datapoint.

In this subsection we will briefly review the results before discussing their implications later.

Table 4. Properties of our simulated clusters. From left to right, the cluster name, number of stars, morphology, fractal dimension (D) when relevant, the half-mass radius ($r_{1/2}$) or fractal radius (r_F), initial virial ratio Q, initial binary fraction, and the symbol for the simulation in Figs. 17, 18, 19, 20, 21 and 22.

Cluster	N_{stars}	Morphology	D	$r_{1/2}$ or r_F	Q	f_{bin}	symbol
ONC	1500	Plummer	-	0.1 pc	0.5	100 per cent	×
ONC	1500	Plummer	-	0.4 pc	0.5	field-like	◇
ONC	1500	Plummer	-	0.8 pc	0.5	field-like	★
ONC	1500	Fractal	2.0	1 pc	0.3	100 per cent	▲
ONC	1500	Fractal	2.0	1 pc	0.3	73 per cent	●
ONC	1500	Fractal	2.0	1 pc	0.3	field-like	■
IC348	260	Plummer	-	0.1 pc	0.5	100 per cent	×
IC348	260	Plummer	-	0.4 pc	0.5	field-like	◇
IC348	260	Plummer	-	0.8 pc	0.5	field-like	★
IC348	260	Fractal	2.0	1 pc	0.3	100 per cent	▲
IC348	260	Fractal	2.0	1 pc	0.3	73 per cent	●
IC348	260	Fractal	2.0	1 pc	0.3	field-like	■
Oph	300	Plummer	-	0.1 pc	0.5	100 per cent	×
Oph	300	Plummer	-	0.4 pc	0.5	field-like	◇
Oph	300	Plummer	-	0.8 pc	0.5	field-like	★
Oph	300	Fractal	2.0	1 pc	0.5	100 per cent	△
Oph	300	Fractal	2.0	1 pc	0.5	73 per cent	○
Oph	300	Fractal	2.0	1 pc	0.5	field-like	□
Cham I	200	Fractal	1.6	3 pc	0.5	100 per cent	△
Cham I	200	Fractal	1.6	3 pc	0.5	73 per cent	○
Cham I	200	Fractal	1.6	3 pc	0.5	field-like	□
Taurus	300	Fractal	1.6	10 pc	0.5	100 per cent	△
Taurus	300	Fractal	1.6	10 pc	0.5	73 per cent	○
Taurus	300	Fractal	1.6	10 pc	0.5	field-like	□

5.6.1 The ONC

In Fig. 17 we plot the binarity in the range 62 – 620 au as a function of density within 0.25 pc of the centroid of the cluster. As can be seen, none of the simulations are perfect fits, but none are terribly bad fits either. The 73 per cent binary fraction collapsing fractal collapsing fraction just matches the observations.

5.6.2 IC348

In Fig. 18 we plot the binarity in the range 32 – 830 au as a function of density within 0.25 pc of the centroid of the cluster. For IC348 very good fits to the observations are found for (a) a field-like initial binary fraction in a 0.4 pc radius Plummer sphere, or (b) a collapsing fractal with a field-like binary fraction. Simulations with an initially 100 per cent binary fraction are particularly poor fits. The 73 per cent binary fraction collapsing fractal simulation is, again, just consistent with the observations.

5.6.3 Ophiuchus

In Fig. 19 we plot the binarity in the range 18 – 830 au as a function of density within 0.25 pc of the centroid of the cluster. In Ophiuchus, a field-like binary fraction, 0.8 pc radius Plummer sphere and a Q = 0.5 fractal with a 73 per cent binary fraction are both reasonable fits.

5.6.4 Cham I

Fig. 20 shows the binarity in the range 18 – 830 au as a function of density within 0.25 pc of the star with the highest stellar surface density in the cluster. As Cham I is rather clumpy we only model it as a fractal. Neither the 100 per cent or the field-like binary fractions are particularly good fits, but the 73 per cent Q = 0.5 fractal is a rather good fit.

5.6.5 Taurus

Finally, in Fig. 21 we show the binarity in the range 18 – 830 au as a function of density within 1 pc of the star with the highest stellar surface density in the cluster. As with Cham I we only model Taurus as a fractal. In this case, the fractal with 100 per cent initial binary fraction is by far the best fit, but the 73 per cent binary fraction, Q = 0.5 fractal is also consistent with the observations.

6 DISCUSSION

In this paper we wish to address the question of the universality of star formation. In particular we wish to examine if the morphologies, densities and binary fractions (within a given separation range) of the observed clusters can be matched by N-body simulations with statistically the same initial conditions (with only the number of stars varying).
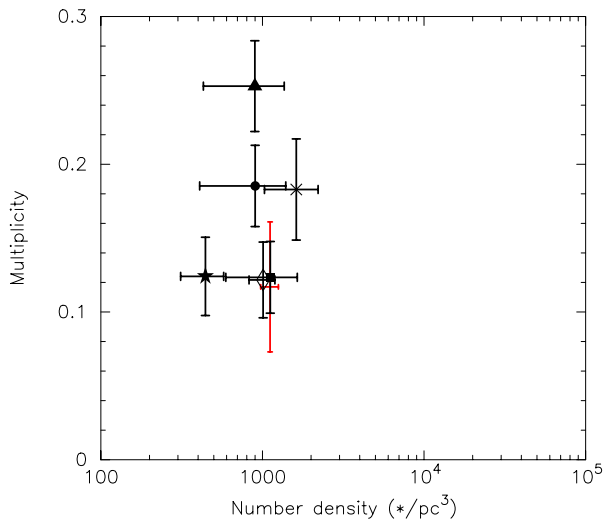
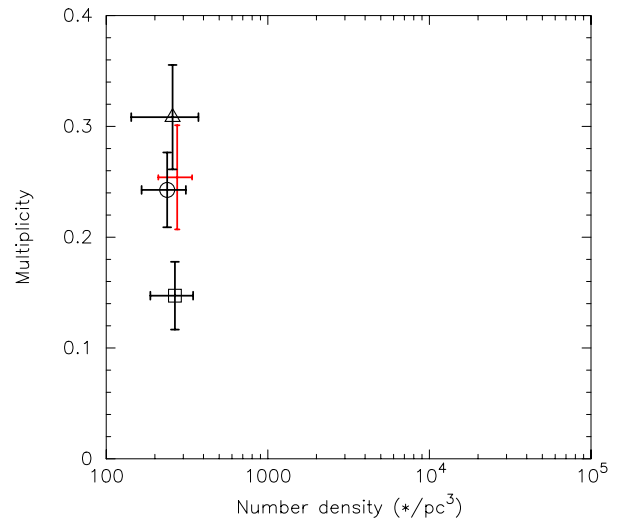We have constructed directly comparable observational
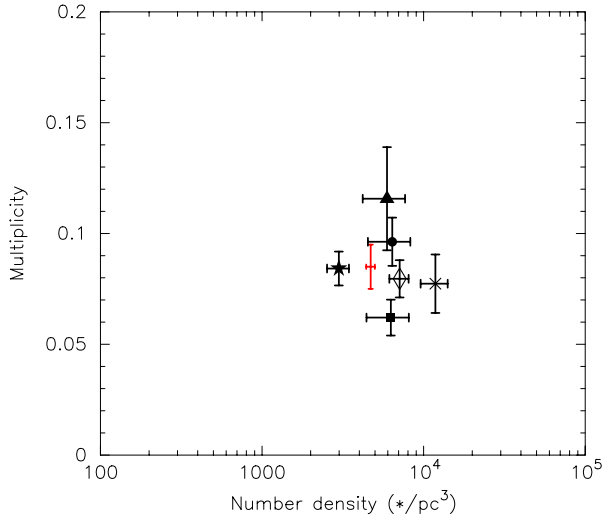
Figure 17. Multiplicity versus stellar density in the separation range 62 – 620 au for various simulated ONC-like clusters (see Table 4 for details). The observed ONC value is shown by the red datapoint.
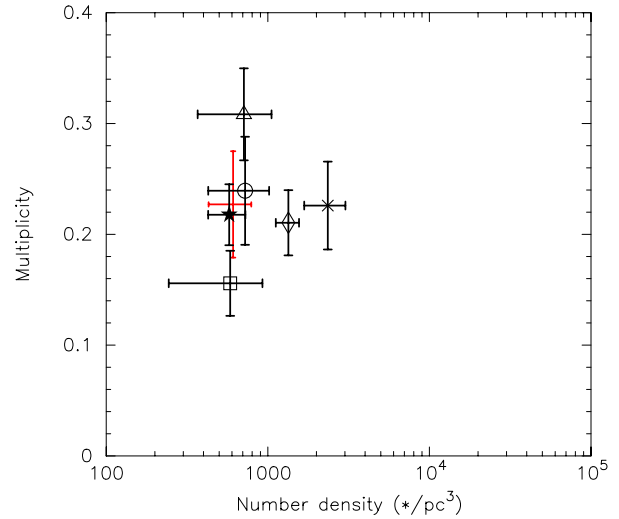
Figure 19. Multiplicity versus stellar density in the separation range 18 – 830 au for various simulated Ophiuchus-like clusters (see Table 4 for details). The observed value in Ophiuchus is shown by the red datapoint.

Figure 18. Multiplicity versus stellar density in the separation range 32 – 830 au for various simulated IC348-like clusters (see Table 4 for details). The observed value for IC348 is shown by the red datapoint.

Figure 20. Multiplicity versus stellar density in the separation range 18 – 830 au for various simulated Chamaeleon-like clusters (see Table 4 for details). The observed value in Chamaeleon I is shown by the red datapoint.

6.1 A single model?

Is there a single model that reproduces all of the observations? The answer is almost, but with several caveats.

The *best* fits for the clusters are all different. The best fits for the ONC and Ophiuchus suggest a fairly large Plummer sphere with an initially field-like binary fraction as the initial conditions. For IC348 a field-like binary fraction is certainly preferred, but with no preference between Plummer or fractal initial conditions. The current state of Taurus and Cham I are clearly clumpy (modelled as fractals, although they may well not be truly fractal) with a clear preference for a 100 per cent binary fraction in Taurus, and a somewhat lower fraction in Cham I.

samples of the binary fractions of Taurus, Cham I, Ophiuchus, IC348, and the ONC. In as far as is possible these samples cover the same physical separation ranges for stars in the same mass range, and with the same companion magnitude differences. Such samples are crucial to ensure we are comparing like-with-like.
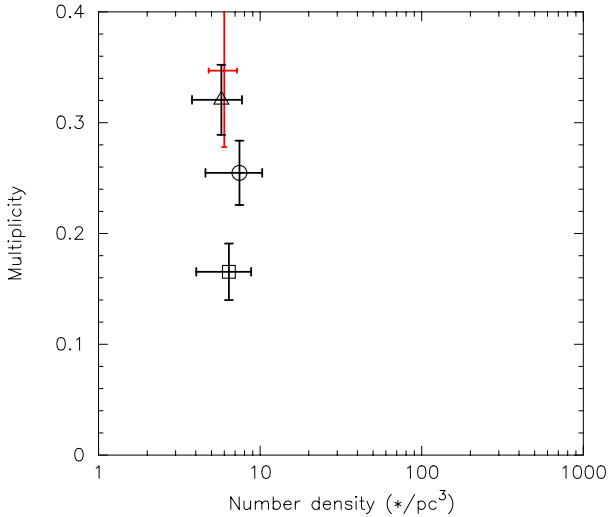
In our simulations we have aimed to start with a wide variety of initial conditions, but to try to match the observed morphologies, densities and binary fractions of the observed clusters at an age of 1 Myr.

Figure 21. Multiplicity versus stellar density in the separation range 18 – 830 au for the simulated Taurus-like clusters (see Table 4 for details). The observed value in Taurus is shown by the red datapoint.
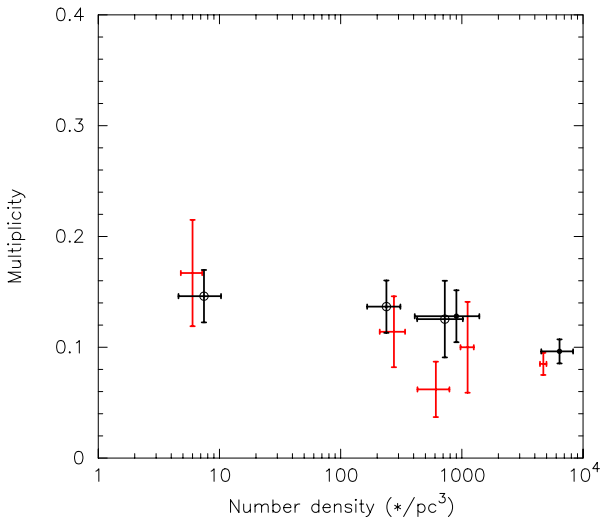
Figure 22. Multiplicity versus stellar density in the separation range 62 – 620 au for all five clusters with a total binary fraction of 73 per cent. The observed values are shown by the red datapoints, the sub-virial clusters shown by filled circles and those in virial equilibrium shown by open circles.

The first thing that we can say is that *a universal model must start with substructure*. Taurus and Cham I are clearly substructured, and so any universal model must also be substructured. However, *a universal model must rapidly erase its substructure* in order to match the fairly uniform appearance of Ophiuchus, IC348, and the ONC.

With numerical experiments we are able to construct a single model that (just) fits all of the clusters (see Fig. 22). This model is fractal with a 73 per cent initial *total* binary fraction. This 73 per cent binary fraction is the initial binary fraction across all separation ranges. Note that we assume that the initial separation distribution is a log normal with $\mu_{\log a}$ = 1.53 and $\sigma_{\log a}$ = 1.57 (i.e. Duquennoy & Mayor

1991 for field G-dwarfs). We will return to a discussion of this assumption later.

However, in order to reproduce the observations we require two different initial virial ratios, $Q = 0.3$ for Ophiuchus, IC348, and the ONC, and $Q = 0.5$ for Taurus and Cham I. The reason for this is that we need to erase substructure in Ophiuchus, IC348, and the ONC (so needing a collapse), but retain substructure in Taurus and Cham I.

This might not be a great problem. We have assumed an age of 1 Myr for all clusters, but this is an approximation. The ONC probably has an age of 2–3 Myr (Mayne & Naylor 2008; Da Rio et al. 2010) and so has had longer to erase its substructure. However, sub-virial clumpy initial conditions are required if we wish to reproduce features of the ONC such as the mass segregation (see Allison et al. 2009).

The fractal dimensions used are also slightly different, $D = 2$ for Ophiuchus, IC348, and the ONC, and $D = 1.6$ for Taurus and Cham I. Higher fractal dimensions begin smoother and so can erase their substructure more easily. Again, we feel that this may not be too great an obstacle to overcome as we did not test many different fractal dimensions. Largely this is because we do not believe the initial distributions to be *truly* fractal, rather the fractal is a useful numerical tool when constructing substructured distributions.

Therefore it might be possible to construct a universal model with high clumpiness (low fractal dimension) close to, but below, virial equilibrium which allows the substructure to be erased rapidly. To be consistent with the clusters discussed here, the initial binary fraction must be high, but not 100 per cent.

Taurus and Cham I present something of a problem for a universal model. Both Taurus and Cham I are substructured and must be dynamically fairly unevolved. However, Cham I has a binary fraction much closer to the presumably dynamically processed Ophiuchus. Is Cham I much more dynamically evolved than Taurus (similar to Ophiuchus), but for some reason has not yet erased its substructure?

6.2 Assumptions about the binary separation distribution

It must be remembered that we are only constrained by observations in the separation range(s) which are observed. For all five clusters we can only compare in the range 62 – 620 au. Rather frustratingly, this range is dominated by 'intermediate' binaries, that is binaries that are neither 'hard' nor 'soft' and whose survival depends on the exact details of the dynamical evolution and if they were 'unlucky' enough to have had a destructive encounter or not. Soft binaries are destroyed within a crossing time (although they may appear and disappear in clusters as they can be re-formed, Moeckel & Clarke 2011). Hard binaries are almost never processed.

Whether an intermediate binary is destroyed, firstly depends on the velocity dispersion of the cluster (which sets the separation range which is susceptible to destruction). It also depends on the encounter probability (itself a function of the velocity dispersion and stellar density) which sets the chance of a destructive encounter occurring. Indeed, in a low enough density environment (such as the field) formally soft binaries can survive as encounters are extremely rare.

Therefore, even though we find that a 73 per cent ini-

tial binary fraction is the best fit, this assumes a G-dwarf field-like log-normal distribution across the whole separation range. Actually the observations tell us nothing about binaries with separations < 62 au or > 620 au in all clusters. Thus our 73 per cent total initial binary fraction corresponds to a ~ 17 per cent initial binary fraction in the range 62–620 au, or ~ 30 per cent in the range 18–830 au. However, outside, and especially below, our observed separation ranges we have no information and the 73 per cent value should be taken with caution. As an extreme example, the ONC *could* have a 100 per cent binary fraction if it had 90 per cent of its stars in 10 au binaries. Observationally, we cannot refute this claim.

7   CONCLUSIONS

We have produced comparable selections of binaries in five clusters: Taurus, Ophiuchus, Cham I, IC348, and the ONC for stars between 0.1 and 3 $M_\odot$. The multiplicity in each cluster has been determined to the same mass limits, mass ratio sensitivity, and within the same separation ranges allowing them to be compared directly with one another. For all five clusters we have multiplicities in the range 62 – 620 au, for all but the ONC we have a range of 32 – 830 au, and for Taurus, Ophiuchus, and Cham I we have a range of 18 – 830 au.

We find in common with previous work that in the range 62 – 620 au Taurus has a significant excess of binaries compared to the ONC (16.7 ± 4.8 per cent versus 8.5 ± 1.0 per cent). We find that the trend of decreasing binary fraction with increasing density is driven solely by the high binary fraction of Taurus. Ophiuchus, Cham I, IC348, and the ONC cover a factor of 17 in density but show no discernable trend. However, we note that a global 'density' is a rather difficult term to define for sub-structured clusters such as Taurus and Cham I.

We perform a large ensemble of *N*-body simulations of Plummer spheres and fractal distributions with different initial (log-normal) binary fractions. We then 'observe' the simulations in the same separation ranges for the same masses and with the same mass ratio sensitivity as the real observations.

We are able to find one set of simulations that roughly reproduce all of the observations: a fractal with a total binary fraction of 73 per cent (albeit with slightly different fractal dimensions and virial ratios). Universal initial conditions must therefore be clumpy as both Taurus and Cham I are clearly not smooth. Universal initial conditions must also have a higher binary fraction in the range 62–620 au than currently observed (in all but Taurus) as dense clusters must process some of their binary population in this range. To test this scenario, binary surveys probing closer separations (~10–60 au) are required.

REFERENCES

Aarseth S. J., Henon M., Wielen R., 1974, A&A, 37, 183
Abt H. A., Gomez A. E., Levy S. G., 1990, ApJS, 74, 551
Allison R. J., Goodwin S. P., 2011, MNRAS, 415, 1967
Allison R. J., Goodwin S. P., Parker R. J., de Grijs R., Portegies Zwart S. F., Kouwenhoven M. B. N., 2009, ApJ, 700, L99
Allison R. J., Goodwin S. P., Parker R. J., Portegies Zwart S. F., de Grijs R., 2010, MNRAS, 407, 1098
Bastian N., Covey K. R., Meyer M. R., 2010, ARA&A, 48, 339
Bressert E., Bastian N., Gutermuth R., Megeath S. T., Allen L., Evans N. J., Rebull L. M., Hatchell J., Johnstone D., Bourke T. L., Cieza L. A., Harvey P. M., Merin B., Ray T. P., Tothill N. F. H., 2010, MNRAS: Letters, 409, L54
Briceño C., Luhman K. L., Hartmann L., Stauffer J. R., Kirkpatrick J. D., 2002, ApJ, 580, 317
Casertano S., Hut P., 1985, ApJ, 298, 80
Da Rio N., Robberto M., Soderblom D. R., Panagia N., Hillenbrand L. A., Palla F., Stassun K. G., 2010, ApJ, 722, 1092
Duchêne G., Bouvier J., Bontemps S., André P., Motte F., 2004, A&A, 427, 651
Duchêne G., Bouvier J., Simon T., 1999, A&A, 343, 831
Duquennoy A., Mayor M., 1991, A&A, 248, 485
Feigelson E. D., Getman K., Townsley L., Garmire G., Preibisch T., Grosso N., Montmerle T., Muench A., McCaughrean M., 2005, ApJSS, 160, 379
Feigelson E. D., Lawson W. A., 2004, ApJ, 614, 267
Fischer D. A., Marcy G. W., 1992, ApJ, 396, 178
Getman K. V., Feigelson E. D., Grosso N., McCaughrean M. J., Micela G., Broos P., Garmire G., Townsley L., 2005, ApJSS, 160, 353
Ghez A. M., McCarthy D. W., Patience J. L., Beck T. L., 1997, ApJ v.481, 481, 378
Ghez A. M., Neugebauer G., Matthews K., 1993, AJ, 106, 2005
Goodwin S. P., 2010, Royal Society of London Philosophical Transactions Series A, 368, 851
Goodwin S. P., Whitworth A. P., 2004, A&A, 413, 929
Güdel M., Briggs K. R., Arzner K., Audard M., Bouvier J., Feigelson E. D., Franciosini E., Glauser A., Grosso N., Micela G., Monin J.-L., Montmerle T., Padgett D. L., Palla F., Pillitteri I., Rebull L., Scelsi L., Silva B., Skinner S. L., Stelzer B., Telleschi A., 2007, A&A, 468, 353
Guieu S., Dougados C., Monin J.-L., Magnier E., Martín E. L., 2006, A&A, 446, 485
Heggie D. C., 1975, MNRAS, 173, 729
Herbig G. H., 1998, ApJ v.497, 497, 736
Hillenbrand L. A., 1997, AJ v.113, 113, 1733
Hillenbrand L. A., Hartmann L. W., 1998, ApJ, 492, 540
Hills J. G., 1975, AJ, 80, 1075

Jeffries R. D., 2007, MNRAS, 376, 1109

Kenyon S. J., Gómez M., Whitney B. A., 2008, Handbook of Star Forming Regions, p. 405

King I. R., 1966, AJ, 71, 64

Köhler R., Leinert C., 1998, A&A, 331, 977

Köhler R., Petr-Gotzens M. G., McCaughrean M. J., Bouvier J., Duchêne G., Quirrenbach A., Zinnecker H., 2006, A&A, 458, 461

Kouwenhoven M. B. N., Brown A. G. A., Portegies Zwart S. F., Kaper L., 2007, A&A, 474, 77

Kouwenhoven M. B. N., Brown A. G. A., Zinnecker H., Kaper L., Portegies Zwart S. F., 2005, A&A, 430, 137

Kouwenhoven M. B. N., Goodwin S. P., Parker R. J., Davies M. B., Malmberg D., Kroupa P., 2010, MNRAS, 404, 1835

Kroupa P., 1995a, MNRAS, 277, 1507

Kroupa P., 1995b, MNRAS, 277, 1491

Kroupa P., 1995c, MNRAS, 277, 1522

Kroupa P., 2002, Science, 295, 82

Kroupa P., 2008, in Aarseth S. J., Tout C. A., Mardling R. A., eds, Lecture Notes in Physics, Berlin Springer Verlag Vol. 760 of Lecture Notes in Physics, Berlin Springer Verlag, Initial Conditions for Star Clusters. pp 181–259

Kroupa P., Petr M. G., McCaughrean M. J., 1999, New Astronomy, 4, 495

Kroupa P., Petr-Gotzens M. G., 2011, A&A

Lada C. J., 2006, ApJL, 640, L63

Lada E. A., Lada C. J., 1995, AJ, 109, 1682

Lafrenière D., Jayawardhana R., Brandeker A., Ahmic M., van Kerkwijk M. H., 2008, ApJ, 683, 844

Leinert C., Zinnecker H., Weitzel N., Christou J., Ridgway S. T., Jameson R., Haas M., Lenzen R., 1993, A&A, 278, 129

Luhman K. L., 2004, ApJ, 602, 816

Luhman K. L., 2007, ApJSS, 173, 104

Luhman K. L., 2008, Handbook of Star Forming Regions, p. 169

Luhman K. L., Allen P. R., Espaillat C., Hartmann L., Calvet N., 2010, ApJ Supplement, 186, 111

Luhman K. L., Mamajek E. E., Allen P. R., Cruz K. L., 2009, ApJ, 703, 399

Luhman K. L., Rieke G. H., 1999, ApJ, 525, 440

Luhman K. L., Stauffer J. R., Muench A. A., Rieke G. H., Lada E. A., Bouvier J., Lada C. J., 2003, ApJ, 593, 1093

Marks M., Kroupa P., Oh S., 2011, MNRAS, accepted, arXiv: 1106.5050

Mason B. D., Gies D. R., Hartkopf W. I., W. G. Bagnuolo J., ten Brummelaar T., McAlister H. A., 1998, AJ, 115, 821

Mason B. D., Hartkopf W. I., Gies D. R., Henry T. J., Helsel J. W., 2009, AJ, 137, 3358

Mayne N. J., Naylor T., 2008, MNRAS, 386, 261

Mayor M., Duquennoy A., Halbwachs J.-L., Mermilliod J.-C., 1992, in McAlister H. A., Hartkopf W. I., eds, IAU Colloq. 135: Complementary Approaches to Double and Multiple Star Research Vol. 32 of ASP Conference Series, CORAVEL Surveys to Study Binaries of Different Masses and Ages. IAU, pp 73–81

Menten K. M., Reid M. J., Forbrich J., Brunthaler A., 2007, A&A, 474, 515

Moeckel N., Clarke C. J., 2011, MNRAS, in press (arXiv: 1103.2306)

Moraux E., Lawson W. A., Clarke C. J., 2007, A&A, 473, 163

Parker R. J., Goodwin S. P., 2011, MNRAS, 411, 891

Parker R. J., Goodwin S. P., Allison R. J., 2011, MNRAS, in press (arXiv: 1108.3566)

Parker R. J., Goodwin S. P., Kroupa P., Kouwenhoven M. B. N., 2009, MNRAS, 397, 1577

Petr M. G., du Foresto V. C., Beckwith S. V. W., Richichi A., McCaughrean M. J., 1998, ApJ v.500, 500, 825

Pfalzner S., Olczak C., 2007, A&A, 475, 875

Plummer H. C., 1911, MNRAS, 71, 460

Portegies Zwart S. F., McMillan S. L. W., Hut P., Makino J., 2001, MNRAS, 321, 199

Portegies Zwart S. F., Makino J., McMillan S. L. W., Hut P., 1999, A&A, 348, 117

Prosser C. F., Stauffer J. R., Hartmann L., Soderblom D. R., Jones B. F., Werner M. W., McCaughrean M. J., 1994, ApJ, 421, 517

Raghavan D., McMaster H. A., Henry T. J., Latham D. W., Marcy G. W., Mason B. D., Gies D. R., White R. J., ten Brummelaar T. A., 2010, ApJSS, 190, 1

Ratzka T., Köhler R., Leinert C., 2005, A&A, 437, 611

Reggiani M. M., Meyer M. R., 2011, ArXiv e-prints: 1106.3064

Reipurth B., Guimarães M. M., Connelley M. S., Bally J., 2007, AJ, 134, 2272

Reipurth B., Zinnecker H., 1993, A&A, 278, 81

Sánchez N., Alfaro E. J., 2010, in IAU Symposium Vol. 266 of IAU Symposium, The spatial distribution of stars in open clusters. pp 524–527

Schmeja S., 2011, AN, 332, 172

Siess L., Dufour E., Forestini M., 2000, A&A, 358, 593

Simon M., Chen W. P., Howell R. R., Benson J. A., Slowik D., 1992, ApJ, 384, 212

Simon M., Ghez A. M., Leinert C., Cassar L., Chen W. P., Howell R. R., Jameson R. F., Matthews K., Neugebauer G., Richichi A., 1995, ApJ, 443, 625

Strom S. E., Strom K. A., Carrasco L., 1974, PASP, 86, 798

Wichmann R., Bastian U., Krautter J., Jankovics I., Rucinski S. M., 1998, MNRAS, 301, L39

Wilking B. A., Gagné M., Allen L. E., 2008, Handbook of Star Forming Regions, p. 351